Cell. Mol. Life Sci. (2011) 68:3403–3423
DOI 10.1007/s00018-011-0636-3

Cellular and Molecular Life Sciences

RESEARCH ARTICLE

Pigment-dispersing hormone in *Daphnia* interneurons, one type homologous to insect clock neurons displaying circadian rhythmicity

Johannes Strauß · Qian Zhang · Peter Verleyen · Jurgen Huybrechts · Susanne Neupert · Reinhard Predel · Kevin Pauwels · Heinrich Dircksen

Received: 20 October 2010 / Revised: 29 January 2011 / Accepted: 1 February 2011 / Published online: 2 March 2011

Abstract We report identification of a beta-type pigment-dispersing hormone (PDH) identical in two water flea species, *Daphnia magna* and *Daphnia pulex*. It has been identified by cloning of precursors, chromatographic isolation from tissue extracts followed by immunoassays and de novo-mass spectrometric sequencing. The peptide is restricted to a complex system of distinct interneurons in the brain and visual ganglia, but does not occur in neurosecretory cells projecting to neurohemal organs as in decapod crustaceans. Thirteen neuron types individually identified and reconstructed by immunohistochemistry were almost identical in terms of positions and projection patterns in both species. Several neurons invade and form plexuses in visual ganglia and major brain neuropils including the central body. Five neuron types show contralateral pathways and form plexuses in the lateral, dorsal, or postlateral brain neuropils. Others are local interneurons, and a tritocerebral neuron connects the protocerebrum with the neuropil of the locomotory second antenna. Two visual ganglia neuron types lateral to the medulla closely resemble insect medulla lateral circadian clock neurons containing pigment-dispersing factor based upon positional and projectional criteria. Experiments under 12:12 h light/dark cycles and constant light or darkness conditions showed significant circadian changes in numbers and activities of one type of medulla lateral PDH neuron with an acrophase in the evening. This simple PDH system shows striking homologies to PDH systems in decapod crustaceans and well-known clock neurons in several insects, which suggests evolutionary conservation of an ancient peptidergic interneuronal system that is part of biological clocks.

Keywords Pigment-dispersing hormone · Circadian clock · Interneuron · Crustacea · *Daphnia magna* · *Daphnia pulex*

Electronic supplementary material The online version of this article (doi:10.1007/s00018-011-0636-3) contains supplementary material, which is available to authorized users.

J. Strauß · H. Dircksen (✉)
Department of Zoology, Stockholm University,
Svante Arrhenius väg 18A, 10691 Stockholm, Sweden
e-mail: dircksen@zoologi.su.se

Q. Zhang
Dr. Senckenbergische Anatomie, Institute of Anatomy II,
J.-W. Goethe-University of Frankfurt, Frankfurt, Germany

P. Verleyen · J. Huybrechts · K. Pauwels
Department of Biology, K. U. Leuven, Leuven, Belgium

S. Neupert · R. Predel
Institute of General Zoology and Animal Physiology,
Friedrich-Schiller-University, Jena, Germany

Abbreviations

$a2n_1$	Second antenna nerve 1
BrOG	Brain-optic ganglia complex
CCAP	Crustacean cardioactive peptide
CEC	Circumesophageal commissure
CHH	Crustacean hyperglycemic hormone
CID	Collision-induced dissociation
CB	Central body
CN	Central neuropil
CNS	Central nervous system
CT	Circadian time
DAPI	4′,6′ Diamino-2-phenylindole-2 HCl
DD	Constant darkness condition
DN	Dorsal neuropil
DVM	Diel vertical migration

ELISA	Enzyme-linked immunosorbent assay
EPR	Extra-retinal photoreceptor
EST	Expressed sequence tag
HPLC	High-pressure lipid chromatography
IEP	Isoelectric point
IIF	Indirect immunofluorescence
La	Lamina
LD	Light dark conditions
LL	Constant light condition
l-LN_vs	Large ventral lateral neurons
LN	Lateral neuropil
MALDI-TOF	Matrix-assisted laser desorption/ ionization-time of flight
Me	Medulla
Mel	Medulla lateral neurons
MLL	Levator labri muscle
NE	Nauplius eye
ORF	Open-reading frame
PAP	Peroxidase anti-peroxidase
PB	Protocerebral bridge
PCN	Precentral neuropil
PDF	Pigment-dispersing factor
PDH	Pigment-dispersing hormone
pec	Post-esophageal commissure
PER	*Period* gene product
PLN	Postlateral neuropils
PPRP	PDH-precursor-related peptide
RACE	Rapid amplification of cDNA ends
RPCH	Red pigment-concentrating hormone
RT	Room temperature
RT-PCR	Reverse transcription-polymerase chain reaction
s-LN_vs	Small lateral ventral neurons
SP	Signal peptide
VNC	Ventral nerve cord
ZT	Zeitgeber time

Introduction

Pigment-dispersing hormones (PDHs) are chromatophore-activating hormones in Crustacea responsible for light adaptation of the eyes and color changes within epidermal chromatophores to adapt to the background [1, 2]. PDHs are octadecapeptides that show antagonistic effects to red-pigment concentrating hormone (RPCH), not only on pigment movements in the eye, but generally on several chromatophores [2]. Similar peptides in insects show high degrees of sequence identity with beta-PDHs, the most common crustacean isoforms. These peptides have been called pigment-dispersing factors (PDFs) since they can elicit chromatophore movement in crustaceans [1, 3, 4]. A dual function for PDHs as neurotransmitters and/or neuromodulators has been suggested by immunocytochemical studies. PDH-ir neurons not only occur in all eyestalk neuropils [5–7] but also in the entire central nervous systems of decapod [8, 9] and isopod [10] crustaceans. A study on lobster embryos [9] identified PDH neurons in the eyestalk, brain, and ventral nerve cord (VNC) with striking similarities to those of crab and crayfish. Several neurons associated with the visual ganglia share multiple putatively homologous characters with insect PDF neurons.

PDFs in insects act as circadian clock output factors that regulate clock neurons [11–13], activity phases, and photoresponsiveness during early night [14]. In *Drosophila melanogaster,* the lateral PDF neurons adjacent to the optic lobe are known to express the *period* gene product, PER [11, 15, 16], which occurs in crustaceans as well [17]. PDF expression in some insects is under control of *period*, *timeless*, and other major clock genes, although, in *Drosophila,* the level of PDF mRNA itself does not display a circadian change in clock neurons [18, 19]. However, in several insects, PDF and e.g., PER are not co-localized [14, 19]. In the crayfish brain, extra-retinal photoreceptors are responsible for the entrainment of circadian locomotory activity. They most likely couple to descending PDH-ir brain interneurons thought to drive motor neurons in the VNC. The intensities of PDH-ir fluorescence staining correlate with changes in the peak locomotor activities after the beginning of the light and dark phases, respectively. Although this system is necessary and sufficient for light entrainment, the main endogenous rhythm generator likely resides in the eyestalk ganglia [20].

Limited information is available about chromatophorotropic hormones in Branchiopoda. Ståhl [21] found in heterologous bioassays that extracts from the brain of *Artemia salina* caused contraction of the colored pigment of the chromatophores of eyeless *Palaemon adspersus*. Although melanin pigment is present at least in the eye of *Daphnia magna* [22] and *Artemia salina* [23], true chromatophores are probably lacking in Branchiopoda [24]. Therefore, we investigated whether PDH or PDF homologues with neurohormonal and/or neuromodulatory roles comparable to those in decapods and insects exist in entomostracan crustaceans, and whether PDH-expressing interneurons participate in crustacean circadian clock control [17]. Recent analyses of expressed sequence tag (EST) data have suggested the existence of an unusual PDH-like peptide in *Daphnia pulex* [25].

The genomes of the species *D. pulex* and *D. magna* are both finished soon, and the former is now an established model organism for studying many aspects of crustacean ecology and physiology ([26, 27]; http://www.nih.gov/science/models/daphnia/). *D. magna* is a key test organism

for water quality and industrial sewage disposals in standardized environmental risk assessment tests [28, 29], because it is sensitive to ecotoxicologically relevant or endocrine-disrupting pollutants that harm higher animals and humans [30, 31]. Nonetheless, little is known about the endocrine system of *Daphnia* except for sites of presumed neurosecretion, as detected earlier by histological methods [32–34]. However, neurohormones similar to decapod crustacean hyperglycemic hormones (CHH [35]) and crustacean cardioactive peptide (CCAP), known in many decapods for their important roles in controlling metabolism and growth by moulting, have been localized in *D. magna* [36–39], and ESTs from *D. pulex* [25] predict the presence of even more decapod-like hormones. CHH neurons in *D. magna* and *Artemia salina* do not occur in typical decapod-like X-organ-sinus gland (XOSG) neurosecretory pathways. Instead, merely CHH-ir interneurons are seen in similar brain positions. The only prominent CHH-ir neurosecretory cells are of peripheral origin projecting to dorsal putative neurohemal areas in the thoracic VNC [37].

We studied the PDHs in two *Daphnia* species and detected their occurrence in interneurons only, as is almost exclusively the case in insects. Biochemical identification and molecular cloning proved an identical primary structure of a novel PDH and extremely similar precursor structures in the two isogenic species *D. magna* and *D. pulex*. The peptide is distributed only in complex interneurons in brain and visual ganglia that are almost identical in both species. None of them is associated with neurohemal organs. We show for the first time that two types of PDH neurons next to the *Daphnia* visual ganglia show striking similarities to decapod PDH- and insect PDF neurons, one type of which shows a clear-cut endogenous circadian rhythm of activity.

Materials and methods

Animals, tissue preparations, and light conditions

A clone of *D. magna* generously supplied by Dr. Bernd Elendt, Badische Anilin- und Soda-Fabrik SE, Ludwigshafen, Germany, was reared in the laboratory in tap water (de-chlorinated by air bubbling) at room temperature under natural light conditions. Other clones of *D. magna* (Straus 1820) (environmental pollution test strain "Klon 5" from the State office for nature, environment, and customer protection North-Rhine Westfalia, Bonn, Germany; originally from the Federal Environment Agency, Berlin, Germany), and *Daphnia pulex* (Leydig 1860) (strain Livpu01, Dept. Biology, Leuven University, Leuven, Belgium; clone originally hatched from resting eggs from a natural population at Brown Moss, North Shropshire, UK) were used for immunohistochemistry, mass spectrometry, and sequencing. Animals were fed ad libitum green algae *Scenedesmus subspicatus* (Chodat 1926:222) or *Scenedesmus obliquus* (Kützing 1833:609) reared under normal daylight in a culture medium (DIN 38412-9.1). Adult parthenogenetic females only were collected for experiments. For immunohistochemistry on whole-mount preparations, the dissection of nervous tissues from animals cold-anaesthetized on ice was carried out in ice-chilled original or calcium-free saline [40] or directly in ice-chilled 4% sodium phosphate-buffered paraformaldehyde containing picric acid fixative (4pFAPA; [41]). Brains were dissected by cutting off the thorax and abdomen and removing the esophagus, gut, and glands from the head capsule. The preparations of entire heads were then left for another 4 h to overnight at room temperature (RT) in the fixative. For paraplast embedding as described previously [42], tissues were fixed for 24 h in Boer's fixative [43] or for 4 h in 4pFAPA at RT.

Controlled light conditions were maintained by keeping animals in a room with a fixed 12:12 light–dark (LD) rhythm, or under constant light (LL) or darkness (DD) regimes, respectively. The light intensity was 300 Lux. Prior to the experiments, the animals were entrained to the respective LD regime for at least 10 days. To sample time-dependent changes in PDH-ir, the animals were collected from the culture at 15 min before the respective Zeitgeber time, cold-anaesthetized on ice and dissected within the next 45 min. After collections from the controlled culture, the rest of the animals were kept continuously under the respective light or dark conditions. Heads were then fixed for 12 h in 4pFAPA, and IIF-labeled as outlined below.

RNA preparation, RT-PCR, and cloning

Total RNA from batches of 50 entire *D. magna* or *D. pulex* snap-frozen and pulverized using mortar and pestle in liquid nitrogen was isolated via the Trizol method according to the manufacturer's instructions (Invitrogen). Preparation of cDNA for 5′- and 3′ rapid amplification of cDNA ends (RACE) was accomplished from ca. 1-10 µg of total RNA using the SMARTer PCR cDNA Synthesis kit (Clontech-Takara, BD Biosciences). Similar total RNA preparations served for other reverse transcription-polymerase chain reactions (RT-PCRs) and further 3′RACE approaches. The RTs were carried out by use of either Superscript II reverse transcriptase (Invitrogen) and an oligo-dT-adapter (5′-GCTGTCAACGATACGCTACGTA ACGGCATGACAGTGT$_{18}$V-3′), or Moloney murine leukemia virus (MMLV)-reverse transcriptase (Promega) and an oligo-dT anchor primer (5′-GACCACGCGTATCGAT GTCGACT$_{16}$V-3′) for 50 min for both at 42°C followed by

an inactivation for 15 min at 72°C and cooling on ice. Thermostable DNA polymerase (GoTaq green kit, Promega, or Advantage2 PCR kit, Clontech-Takara) was used as recommended in the manufacturer's instructions under conditions especially for RACE approaches and using primers as detailed in Supplementary table 1. For PCRs other than RACE-PCR the following conditions for a touch-down PCR were followed: 94°C for 2.5 min, five cycles of 94°C for 0.5 min, 72°C for 1.5 min, five cycles of 94°C for 0.5 min, 70°C for 1.5 min, 26 cycles of 94°C 1 min, annealing at 58–65°C depending on the primers for 0.5–1 min, elongation at 72°C for 0.5–2 min and finally for 6-9 min depending on the product length. PCR products obtained with primers as listed in Supplementary table 1 were purified from excised gel pieces (QIAEX II gel purification kit, Qiagen) and sequenced directly or after cloning into pGEMT-easy vector and transfection into in JM109 competent *E. coli* (Promega). Clones containing the insert were isolated and grown overnight. Plasmid DNA was purified (GFX Micro Plasmid prep kit, Amersham) and the inserts were sequenced. DappuPDH-specific primers were constructed according to available genomic and EST information (http://genome.jgi-psf.org/cgi-bin/dispGeneModel?db=Dappu1&id=306549; EST: FE404659). While initial attempts using degenerate primers directed towards the conserved peptide parts encoded on the DappuPDH mRNA sequences were unsuccessful, assuming sufficient sequence similarity for use of DappuPDH-specific primers led to success in obtaining a short sequence of the DapmaPDH ORF in the very first step. The next steps used overlapping 5′-and 3′-RACE approaches on the above-mentioned cDNAs according to the manufacturer's instructions. The schematic cloning strategy is depicted in Supplementary Fig. 1. For sequence and bioinformatic analyses, Vector NTI v.9.0.0 (Informax/Invitrogen) or BioEdit v.7.0.5.3 [44] were applied.

Chromatography and enzyme-linked immunosorbent assay

Dissection of tissues was carried out in ice-chilled saline [40]. Heads of the animals were cut with fine scissors through the mandibular segment just caudally from the second antennae, which had been severed previously. Carefully dissected brain-optic ganglia (BrOG) complexes in some cases with adhering cuticle were transferred into ice-cold 2 M acetic acid. The remaining ventral bodies were placed separately in the same extraction medium. Tissues were homogenized by sonication (Branson sonifier) for three times 30 s and centrifuged at 12,000 g. Then the supernatants were transferred into HPLC-Minisorb tubes (NUNC-Thermo Fisher, Roskilde, Denmark), fresh acetic acid was added in the cases of the BrOGs, and the pellets were re-extracted twice. In the cases of the ventral bodies, 80% aqueous methanol was used instead of acetic acid for the two additional re-extraction steps. All extract supernatants were first subjected to a Sep-Pak-C18 (Waters, Milford MA, USA) pre-purification before chromatography on a reversed phase HPLC system (Waters). The system consisted of two type 510 pumps, a model 680 solvent programmer, an U6 K injector, a model 481 LC spectrophotometer (all Waters) and a chart recorder (Perkin-Elmer recorder 56) or alternatively an integrator (Waters 740 Data Module). Solvents for gradient elution were 0.11% trifluoro acetic acid (TFA) in H_2O (A) and 60% acetonitrile (MeCN) in 0.10% TFA (B) in water. A linear gradient of mixtures of solutions A and B from 30 to 80% solution B within 60 min was applied to a μ-Bondapak Phenyl column (Waters) with a flow rate of 0.9 ml/min. Individual peak fractions monitored at 210 nm were collected manually, completely dried in a vacuum centrifuge and analyzed by a sandwich ELISA as described previously [45], Fig. 1d.

MALDI-TOF and MALDI-TOF-TOF mass spectrometry

Mass spectrometric investigations were made of neuropeptides in ice-cold 1 M acetic acid extracts of *D. magna* and *D. pulex* BrOGs. After collection, the samples were homogenized using ultra-sound and centrifuged to remove all cell components from the extract. The supernatant was concentrated to near dryness in a vacuum centrifuge (Speed-Vac, Savant) and subsequently pre-purified on ZipTip-C18 (Millipore) micro-cartridges. The retained peptides were eluted with 60% MeCN/0.1% TFA solution for direct application and mixing with matrix on the target plate. MALDI-TOF–MS was performed on a Reflex IV instrument (Bruker Daltonics, Bremen, Germany), equipped with an N_2 laser (337 nm) and pulsed ion extraction accessory. The instrument was operated in the positive ion, reflectron mode, and calibrated using a standard peptide mixture containing angiotensin II (1,045.54 Da), angiotensin I (1,295.68 Da), substance P (1,346.73 Da), bombesin (1,618.82 Da), ACTH Clip 1–17 (2,092.08 Da), and ACTH Clip 18–39 (2,464.19 Da) (Bruker Daltonics). The instrument settings were as follows: ion source 1, 25.00 kV; ion source 2, 20.35 kV; pulsed ion extraction set at 200 ns; lens voltage, 12.30 kV; and reflector voltage, 28.70 kV. Matrix deflection was set at 500 Da and the laser energy was adjusted to just above desorption/ionization threshold. Spectra were recorded in the reflectron mode within a mass range from *m/z* 500–3,000 and are the results of ca. 100 shots.

For direct tissue profiling of small pieces of the brain known to contain PDH-expressing neurons, *D. magna* as

well as *D. pulex* were fixed with micro-needles and submerged in an insect saline (pH 7.25) of the following composition: NaCl (7.50 g/l), KCl (0.20 g/l), $CaCl_2$ (0.20 g/l), and $NaHCO_3$ (0.10 g/l). The heads were opened with fine forceps and ultra-fine scissors, the brains dissected and subsequently cut in smaller pieces, which were transferred with a glass capillary into a drop of distilled water on the sample plate for MALDI-TOF mass spectrometry. The water was removed using the same glass capillary. The tissues were air-dried and covered with approximately 50 nl (depending on the sample size) of matrix solution (saturated alpha-cyano-4-hydroxycinnamic acid dissolved in methanol/water (1:1) over a period of about 5 s using a Nanoliter injector (World Precision Instruments, Berlin, Germany). Each preparation was air-dried again and finally covered with distilled water for a few seconds, which was finally removed with cellulose paper, to reduce salt contents. MALDI-TOF analyses were performed on an ABI 4800 Proteomics Analyzer (Applied Biosystems, Framingham, MA, USA). In order to determine the parent masses, the instrument was initially operated in reflectron mode. For the tandem MS experiments (performed in gas-off mode), a CID acceleration voltage of 1 kV was used in all cases. The number of laser shots used to obtain a spectrum varied from 800 to 4,000, depending on signal quality. The fragmentation patterns were analyzed by use of the Data ExplorerT software 4.3 package to manually determine the sequence of the peptide.

Antisera, immunocytochemistry, and controls

A rabbit antiserum against synthetic *Uca*-PDH (= beta-PDH, [5]; code 3B3) was used that has been scrutinously characterized for epitope specificity in several previous studies on crustaceans and insects [5, 45, 46]. For indirect immunofluorescence (IIF) staining of whole-mount preparations, tissues were washed in 0.01 M sodium phosphate buffer, pH 7.4, containing 0.9% NaCl and 0.02% sodium azide (PTXN) and incubated with anti-PDH-serum diluted 1:16,000 to 1:24,000 overnight at RT followed by fluorescein-isothiocyanate-labeled goat anti-rabbit IgG (FITC-GAR, Sigma, Taufkirchen, Germany) diluted 1:50–1:80 in PTXN for 1 h in darkness at RT. In some preparations, a 10 µg/ml DAPI solution (4′,6′ diamino-2-phenylindole-2 HCl, Invitrogen) in 0.01 M sodium phosphate-buffered saline (PBS, pH 7.4) was used for 10 min at RT for counter staining of nuclei. The peroxidase anti-peroxidase (PAP)-staining method [47] was performed as described previously on conventional 5-7-µm-thick serial Paraplast sections [48]. These were incubated with anti-PDH-serum diluted 1:5,000 with PTXN for 12–16 h. After extensive washes in PTXN, sections were sequentially incubated with goat anti-rabbit serum (GAR, Biogenzia Lemania, Bochum, Germany) diluted 1:30 in PTXN, with PBS wash without sodium azide and PAP (Biogenzia-Lemania, Bochum, Germany) diluted 1:300 with PBS for 1 h, all procedures carried out at RT. The peroxidase reaction was carried out under visual control for about 5 min with 0.05% 3,3′-diaminobenzidine tetra-hydrochloride (DAB, Sigma–Aldrich) and 0.002% hydrogen peroxide (Merck, Darmstadt, Germany) as substrate in 0.05 M Tris–HCl buffer, pH 7.6, containing 0.9% NaCl. PAP-stained sections were dehydrated in graded alcohol series, cleared in methyl benzoate and mounted in DePeX (Merck). In total, more than 150 whole-mounts and ten Paraplast section preparations were examined for PDH-immunoreactivity.

Preabsorption controls were carried out by pre-incubation of primary antisera with an excess of synthetic *Uca*-beta-PDH (generous gift of Dr. S.G. Webster, Bangor, North Wales, UK) for 24 h at RT prior to immunocytochemical staining. Treatments with 10 nmol *Uca*-PDH calculated per 1 µl undiluted anti-PDH-serum but added to its final dilution completely abolished immunostaining.

Documentation, morphometry, and statistics

IIF-stained preparations were mounted in 80% glycerol containing 50 mg/ml DABCO (1,4-diaza-bicyclo [2.2.2]-octane, Fluka) and viewed under a Leitz Orthoplan fluorescence microscope equipped with a Hg-epi-illumination system and an I2 filter system, or with a Zeiss Axioscope equipped with differential interference contrast optics, epifluorescence, or a Zeiss Axioplan2 epifluorescence microscope equipped with an Axiocam digital camera, computer-controlled by Zeiss Axiovision 4.3 software, allowing for merging and smoothing of several focus planes (extended focus module). Some of the best IIF preparations received additional PAP staining to achieve permanent preparations (for details see [48]). Tracings of neurons were made with the aid of camera lucida attachments to the Leitz Orthoplan or a Zeiss Standard microscope. IIF specimens were imaged with a Zeiss LSM510 Meta (Zeiss, Jena, Germany) laser-scanning confocal microscope. Confocal images were obtained at an optical section thickness of 0.5, 1.5 and 3 µm and were processed with Zeiss LSM Confocal Software. Scanned photographic and digital microscope images were finally adjusted slightly for contrast or brightness in Corel Photopaint 11.0 or Adobe Photoshop 6.0 and assembled with Corel Draw 11.0.

Quantifications of diurnal changes in PDH-immunofluorescence were done on pictures taken with the same Zeiss Axioplan2 microscope as described above. To guarantee comparability of measurements from different preparations, all photographs were taken at a fixed exposure time of 1,243.96 ms and with identical microscope settings with regard to 40× objective and 16× magnifications. Numbers of PDH-immunopositive cells were counted for $n = 12$

specimens. All obtained values refer to the number of neurons per hemiganglion in a given preparation. Fluorescence intensity was quantified from digital images with the NIH ImageJ software (http://rsbweb.nih.gov/ij/) by measuring pixel number on a greyscale ranging from 0 (black) to 255 (white) for the somata by applying a circle of the defined diameter of 45 pixels. Intensity values were determined by subtracting the staining intensity measured for an identical background area immediately adjacent to the soma. A standardized mean intensity value was calculated for the mel1 neurons in a given hemiganglion in order to account for differences in mel1-neuron numbers: the intensity values obtained from individual neurons within one preparation were summed, divided by the number of somata actually present in this preparation, and multiplied by the maximal number of five neurons in the preparations evaluated in this experimental series. The method is modified from [49]. A final staining index was calculated by dividing the resulting values by 10^6. For statistical analysis, Student's *t* test, one-way analysis of variance (ANOVA) with Tukey's multiple comparison test, and two-way ANOVA were performed with the Prism 4 software (Graph Pad Software Inc, La Jolla, CA, USA).

Terminology

For the description of the optic ganglia 1 and 2 (terminology of earlier authors) in our species we have adopted the terminology lamina and medulla of Aramant and Elofsson [50] who, however, omitted some protocerebral neuropils. Thus, the brain neuropil structures serving as landmarks have been termed after Cunnington [51], because this author provided the first comprehensive study and demonstrated conclusively, e.g., on sections, the existence of distinct protocerebral and deutocerebral neuropils in the closely related *Daphnia* species *Simocephalus sima* (formerly called *Daphnia sima*). This study has later been supplemented in the cases of other *Daphnia* species by the novel descriptions of tritocerebral (circumesophageal) neuropils by Leder [52]; see also Supplementary table 2 for synonyms). In our study, however, the latter neuropils have not been considered in any detail since they rarely were associated with distinct PDH-immunoreactive (PDH-ir) structures. For muscles, we adopted the terminology of Binder [53].

Results

Identification of PDH and its gene-derived products in *D. pulex* and *D. magna*

First information on the close similarity of a putative crustacean beta-PDH-like peptide in *D. magna* to a decapod PDH (*Uca*-PDH) was obtained from an HPLC-ELISA approach. No immunopositive HPLC-fraction was found in ventral body extracts, while one fraction from brain/optic ganglia (BrOG) extracts contained a PDH-ir substance eluting close to the retention time of the synthetic *Uca*-PDH standard as revealed by ELISA (Fig. 1a–c). An additional much smaller and earlier eluting immunoreactive peak fraction, also present in the standard (Fig. 1a, c), could, however, not be detected by immunodot-blotting (data not shown). The highest amount of PDH-ir substance was detected in the later eluting fraction (1.26 fmol PDH-

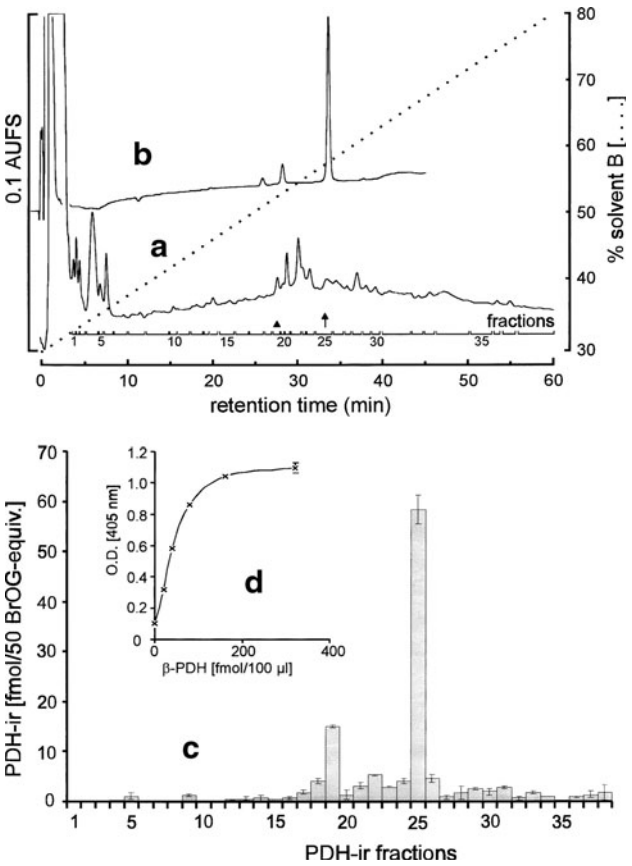

Fig. 1 Immunochemical analysis of PDH-ir substances in HPLC-separated extracts of BrOG complexes of *D. magna*. HPLC chromatograms of a 2 N acetic acid extract of 150 brains of *D. magna* (**a**) and a 1-nmol synthetic *β*-PDH standard (**b**) under identical conditions. Among 38 manually collected peak fractions, one peak shows strongest immunoreactions both in immunodot-blotting and ELISA (*arrow*), and an additional peak is immunopositive only in the ELISA (compare **c**) but not in immunodot-blots (not shown). **c** Fraction 19 but especially fraction 25 of the HPLC in **a** contains the vast majority of PDH-ir material as determined by ELISA per 50 BrOG-equivalents, fraction 25 eluting at a retention time close to that of synthetic *β*-PDH. **d** Measuring range of the corresponding *β*-PDH standard curve. Waters *μ*-Bondapak phenyl column (0.39 × 30 cm) and gradient elution with solvent A: 0.11% TFA and solvent B: 0.10% TFA; 60% acetonitrile (CH_3CN) from 30 to 80% B in 1 h at a flow rate of 0.9 ml/min; *AUFS* absorption units full scale

like material per animal), the smaller preceding peak contained only 0.26 fmol PDH per animal. The retention times of the immunoreactive fractions (Fig. 1a, 27.7 and 33.5 min) closely resemble those found for the synthetic β-PDH standard (Fig. 1b, 28.6 and 33.9 min).

The PDH gene of *D. pulex* is annotated as a two-exon gene (Daphnia Genome Consortium; Joint Genome Institute, http://genome.jgi-psf.org/cgi-bin/dispGeneModel?db=Dappu1&id=306549; predicted mRNA: 1335 bp). We have partially sequenced a corresponding DappuPDH mRNA-precursor of 738-bp encoding an open-reading frame (ORF) of 507-bp length (accession no. HQ843174; Suppl. Fig. 1c). This ORF covers the genomic-predicted ORF and derives a 169-aas-long precursor protein giving rise to a signal peptide (SP) of 28 aas, a long PDH-precursor-related peptide (PPRP, 120 aas) and a novel DappuPDH of 18 aas followed by a single glycine most likely giving rise to its amidation (Fig. 2a, b, Suppl. Fig. 1c). Moreover, we have full-length cloned a similar but shorter PDH-mRNA of 1197 bp from *D. magna* with an ORF of 513 bp in length (Accession No. HQ843173; Suppl. Fig. 1a, b). Compared to the derived DappuPDH precursor, the 170-aa-long DapmaPDH precursor gives rise to a similar SP (71% aa identities) of the same length, and a somewhat more different PPRP (60% identities, 120 aas and 121 aas, respectively). The PDH peptide parts of the mRNA nucleotide sequences are almost identical in both species, showing only conservative single-base exchanges in three positions encoding Leu^{9}, Leu^{11}, Pro^{12}, (and the stop codons) but encoding an identical PDH peptide (Fig. 2b). When analyzing identically processed acetic acid extracts from *D. pulex* and *D. magna* BrOGs, MALDI-TOF mass spectrometry showed an ion signal of $[M + H]^+$: 2,029.20 Da for the predicted DappuPDH and $[M + H]^+$: 2,029.14 Da for the predicted DapmaPDH (calculated 2,029.16 Da) (Fig. 3a). Identical observations were made by direct tissue profiling of the optic lobes of both species (data not shown). By use of tandem mass spectrometry, we further analyzed the ion signals of interest under collision-induced dissociation (CID)-fragmentation (gas-off). The resulting mass spectra contained clear fragments, and the calculation of mass differences between successive fragments of the different ion series allowed to unambiguously reconstruct the following amino acid sequence: NSELINSLLGLPRFMKVV-NH_2 (Fig. 3b). For both species, the predicted identical PDH has thus been confirmed.

Identified PDH-immunoreactive neurons

The *Daphnia* brain consists of the protocerebrum and deutocerebrum, which are located in close association, as well as the tritocerebrum (Supplementary Fig. 2). In the visual system, the left and right compound eyes and the laminae (La) of both sides are completely fused. However, the medullae (Me) are separate ganglia, which are connected to the anterior dorsal and lateral parts of the brain. Among five distinguishable protocerebral neuropils (Suppl. Fig. 2, Fig. 7a, f–h), three are unpaired, the central neuropil (CN), the dorsal neuropil (DN) and the central body

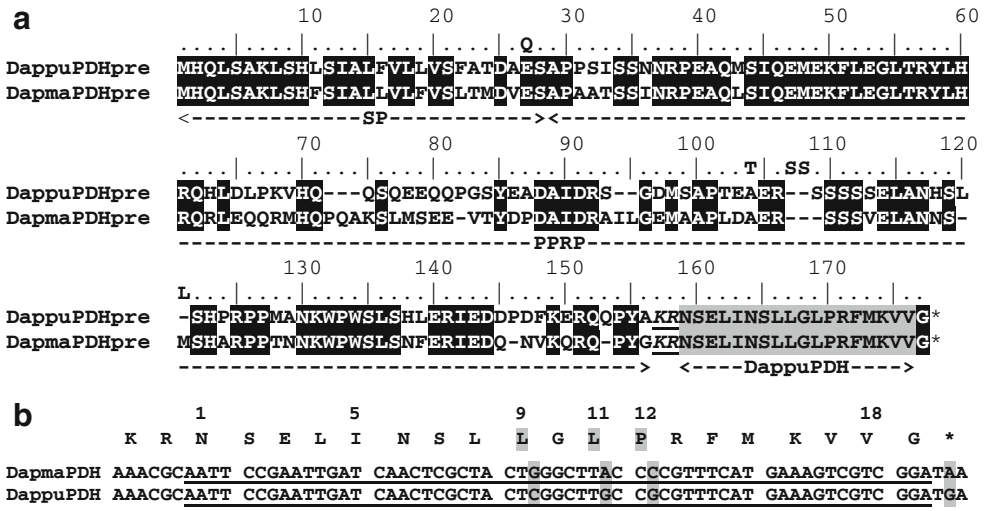

Fig. 2 Comparison of DapmaPDH and DappuPDH precursors derived from the ORFs of the cDNAs (http://genome.jgi-psf.org/cgi-bin/dispTranscript?db=Dappu1&id=306549&useCoords=1), and Suppl. Fig. 1; **a**. Alignment of the DappuPDH- and the DapmaPDH-precursor showing the SPs (both 28 aas long), the PPRPs and the identical novel PDH peptide (18 aas). Note that DapmaPPRP (121 aas) is one aa longer than DappuPPRP (our clones: 120 aas, genomic: 123 aas; compare also Suppl. Fig. 1), and the overall precursor aa-identities are 67%. **b** Part of the ORF-derived precursor nucleotide sequences encoding the peptide after a dibasic (KR) cleavage site; note the four (silent) nucleotide exchanges in the third codon positions only of aas 9, 11, 12, and in the stop codon

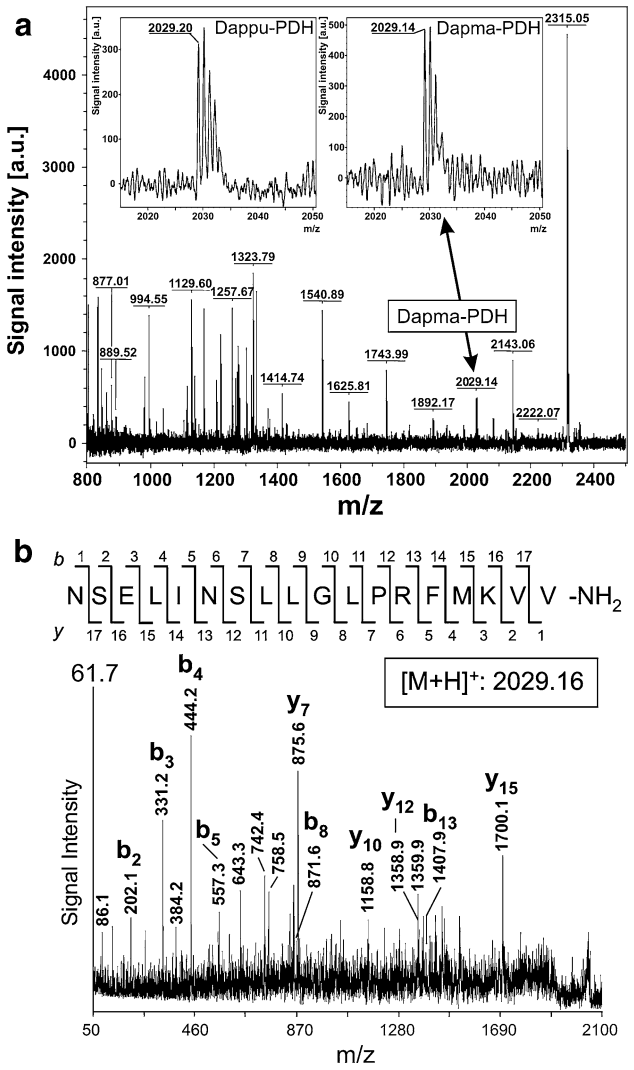

Fig. 3 Identification of DapmaPDH and DappuPDH from a BrOG extract from *D. magna* and *D. pulex* as well as by direct tissue profiling of the optic lobes from both species. **a** Representative MALDI-TOF mass spectrum from the *D. magna* BrOG extract, which contains an ion signal at $[M + H]^+$: 2,029.14 Da identical with the predicted DapmaPDH $[M + H]^+$: 2,029.16 Da. The *insets* show in more detail the same enlarged mono-isotopic ion signal of DapmaPDH (*right*) and a very similar trace at $[M + H]^+$: 2,029.20 Da (*left*) from the *D. pulex* brain extract preparation. **b** CID mass spectrum of PDH (direct tissue profiling of the *D. magna* brain) that confirmed the predicted amino acid sequence of PDH. A number of *y*- and *b*-type fragment ions are labeled

(CB, Figs. 4, 5a–c, 6a, f–h), and two are paired, the lateral and precentral neuropils (LN, PCN; [51]; see supplementary material).

A total of 36–40 immunopositive PDH-ir neurons occur in the visual ganglia, the protocerebrum and the deutocerebrum of *D. magna* and *D. pulex* brain in bilaterally symmetrical arrangement as revealed both in sections and whole-mount preparations (Fig. 4). One PDH-ir neuron has been detected in the tritocerebrum lateral to the esophageal orifice (see below), but none in the VNC or in the peripheral nervous systems. Thus, the results of the immunochemical analyses of brain and ventral body extracts match those obtained by immunohistochemistry. Since numbers and distributions of PDH-ir neuron types are virtually identical in both species with few exceptions (Fig. 5a, b), we have analyzed these neurons in more detail in *D. magna,* but provide distinctions to *D. pulex* where obvious.

In each optic lobe, in total three somata of two clearly distinguishable types of neurons are always found in the dorsal lateral cortical layer of the Me, the medulla lateral (mel) PDH-ir neurons (Figs. 4, 5a–c, 6a).

Type mel1 neuron

This bipolar neuron type comprises two lateral punctate-stained cell bodies, which usually stain so faintly that their axons cannot be traced. However, dependent upon diurnally changing activity (see also below), up to five mel1-cell bodies appear, and their axons can occasionally be detected in evening preparations to enter both the Me and the lateral brain neuropil (Figs. 5a–c, 6a).

Type mel2 neuron

The other type of Me-associated neuron shows rostral and caudal projections from usually T-shaped branches but in several cases exhibits even a bipolar structure. It consistently shows much stronger staining than the mel1 neuron type. The distally projecting axon enters the center of the Me, where fine terminal branches are detectable throughout the entire neuropil. In addition, as has clearly been detectable only in PAP-stained whole-mount preparations, further very faintly stained fibers arising from this branch can be traced to enter tangentially the La neuropil up to its distal parts where they presumably terminate between columnar elements of the pseudo-cartridges as described earlier from Golgi and electron microscopic preparations [54, 55] and more central areas of the La neuropils (Fig. 4). The proximal projection can be traced via the optic nerve tract to terminals profusely branching within the mediosagittal parts of the LN of the protocerebrum (Figs. 4, 5a–c, 6a). Although we could not trace axons beyond this neuropil with certainty, we cannot exclude that one fine fiber continues as a contralateral projection via the CN (Fig. 5c).

In the brain including the tritocerebral part, a total of 11 types of bilaterally symmetrical neurons in ventral and dorsal parts are distinguishable according to their shapes, positions, staining, and projection patterns.

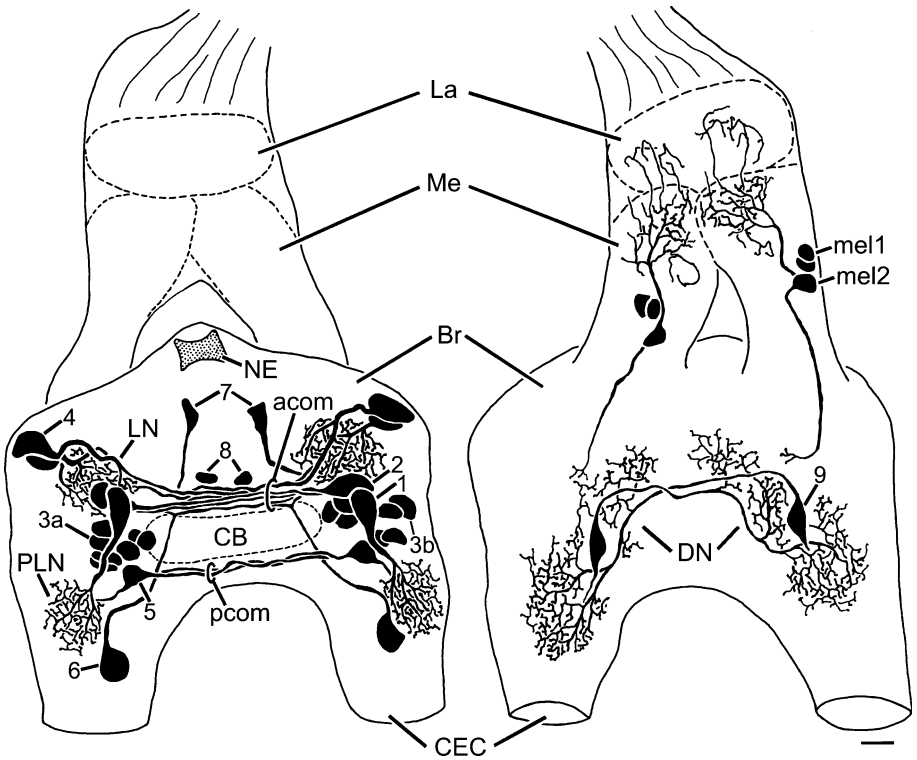

Fig. 4 Camera lucida drawing of PDH-ir neuron types in the optic ganglia (two types; *mel1, mel2*) and the brain (nine types; *1–9*) of *D. magna* (*left* ventral view, *right* dorsal view of the same PAP-stained whole mount). The *mel2* neuron in the medulla (*Me*) connects with T-shaped branches the lamina cartridges and the medulla neuropil with the protocerebral lateral neuropil. Note the fibers in the anterior (*acom*) and posterior (*pcom*) commissures and the terminal arborizations in the lateral and postlateral neuropils (*LN, PLN*) as well as the lateral extension of the dorsal neuropil (*DN*) indicated by arborizations of type-9 neurons. In this preparation, the very faintly staining type-10 neurons, as well as the fine fiber networks within the central body were omitted from the drawing. See Suppl. Fig. 2 for further abbreviations. *Scale bar* 10 μm

Type-1 neuron

The soma of this strongly stained monopolar neuron type lies at the ventral lateral margin of the brain and projects ipsilaterally into the PLN of the deutocerebrum (Figs. 4, 5a–c, 6a), where the axon branches extensively and forms a dense plexus of fine fibers and terminals (Figs. 5a, b, 6b, i).

Type-2 neuron

The perikaryon of this strongly stained monopolar neuron is localized in the ventral lateral part of the brain next to that of the type-1 neuron, but in a slightly more anterior dorsal position (Figs. 4, 5a, b, 6a, c). Its axon runs through the anterior brain commissure (Figs. 4, 5a, b, d, e, 6a, c, d) to the contralateral side, and this projection most likely contributes to terminals in the lateral neuropils.

Type-3 neuron

These cells form a cluster of relatively small monopolar neurons in the ventral lateral brain in a position slightly more posterior or dorsal to type-1 and ventral to type-5 neurons (Fig. 4). Each cluster consists of at least seven cells, which we tentatively subdivide into subtype-3a and -3b. The subtype-3a perikarya characteristically exhibit a weak staining, and their axons are often hardly detectable (Figs. 5a, b, 6a, b, h, i). However, as judged from suitably stained cross sections, at least some of these cells contribute to axons supplying fiber arborizations in the anterior and ventral CB neuropil areas and ipsilateral LNs (Figs. 5d, e, 6d, e, h, i). In some preparations, the subtype-3b neuron is more strongly stained. Its position varies considerably; it usually lies adjacent to the subtype-3a neurons (Fig. 4), but its cell body can even be found at the ventral lateral margin of the brain (Figs. 5a, 6h). When strongly stained, the axons can be followed to additional ipsilateral fiber networks in neuropil areas between the LNs and the PLNs as revealed in more detail only by confocal microscopy (Figs. 5a, c, asterisk).

Type-4 neuron

The somata of the two prominent neurons of this group of strongly immunopositive monopolar neurons with similar branching patterns lie next to each other in an anterior

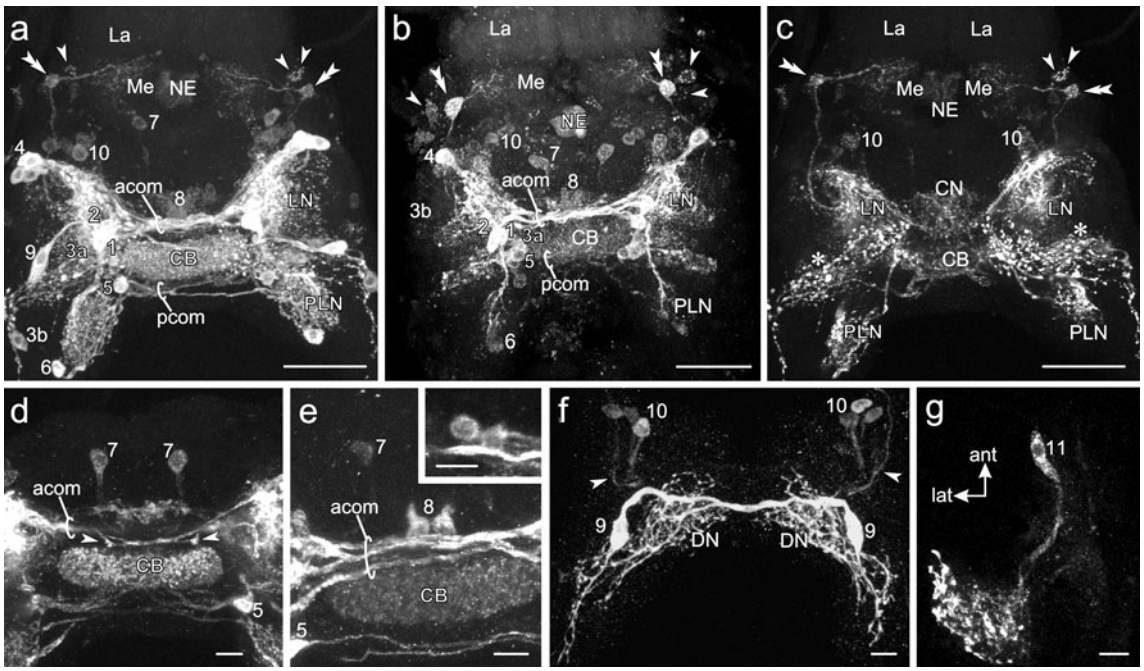

Fig. 5 Confocal micrographs of PDH-ir neurons in the optic ganglia and the brain of *D. magna* (**a**, **c-g**) and *D. pulex* (**b**) in whole-mount IIF-preparations. **a** Overview of all neuron types (stack of 28 virtual sections, 1.5 µm-thick), the two mel1 neurons (*arrowheads*), the T-shaped *mel2* neurons (*double arrowheads)* showing fibers and terminal branches in the medulla (*Me*) and the lamina (*La*). Note the PDH-ir fiber networks in the central body (*CB*) and the axons in the anterior and posterior commissure (*acom*, *pcom*). **b** Similar overview showing the same neuron types as in **a** (stack of 34 virtual sections, 1.5 µm thick). Note the more prominent type-7 neurons. **c** Stack of 30 virtual sections (1 µm thick) showing the medulla-associated neurons (mel1, *arrowheads*; mel2, *double arrowheads*) and the mel2-projections into the lateral neuropils (*LN*); the LN is connected via PDH-ir fibers with the central neuropil (*CN*) and the contralateral LN. Note the positions of the type-10 neurons and the neuropil areas between LN and postlateral neuropils (*PLN*) derived from type-3b neurons (*asterisks*). **d** Type-7 neurons, posterior ventral innervations of the CB derived from type-5 neurons, and branching points (*arrowheads*) of type-6 neurons in the *acom*. **e** Ventral view of paired medial type-8 neurons anterior to the *acom* and their dorsally projecting axons (compare Fig. 7a). *Inset* shows cell bodies with relatively large nuclei and little cytoplasm. **f** Bipolar type-9 neuron in the posterior dorsal protocerebrum with contralateral projections and arborizations of the central axons in the dorsal neuropil (*DN*). Note the projection of the lateral axons in the DN extensions and the position and partial projections of the type-10 neurons, as well as the axons of mel2 neurons (*arrowheads*). **g** Type-11 neuron in the tritocerebrum; note the dense fiber plexus in a posterior lateral neuropil of the tritocerebrum near the entrance of the antennal nerve 1; ant/lat anterior/lateral. *NE* nauplius eye; *PLN* postlateral neuropil. *Scale bars* 50 µm in a–c, 10 µm in d–g

ventral lateral part of the brain. Their axons split into two branches; one contributes ipsilaterally to anterior ventral lateral parts of the LN where it forms plexuses and fine terminal branches (Figs. 4, 5a, b, 6a, b, f), the other runs through the anterior brain commissure into the contralateral LN (Figs. 4, 5a, b, d, e, 6d). In some cases, single faintly stained PDH-ir perikarya occur in positions anterior lateral but just next to the type-4 somata (Fig. 5a) or at the mid-lateral margin of the brain in sagittal sections (Fig. 6b).

Type-5 neuron

This bipolar neuron type showing medium to strong staining intensity is found in the posterior lateral region of the brain close to the ventral lateral edge of the CB (Figs. 4, 5a, b, 6a, h). The lateral axon is projected directly into the PLN, the medial axon runs counter-parallel to the axon of the corresponding neuron of the other side through the posterior commissure of the brain (Figs. 4, 5a, b, 6d, e), but its contralateral termination sites could not be established. Confocal micrographs revealed that the axons give off branches into the CB (Fig. 5d, e). The general branching pattern resembles that of the dorsal bipolar type-9 neuron but on the posterior ventral side of the brain. In *D. pulex* brains, the medial axons of this neuron type in the posterior commissure (Fig. 5b) are usually less prominent than in *D. magna* brains.

Type-6 neuron

The soma of this strongly stained monopolar neuron lies at the posterior ventral lateral margin of the brain next to the tritocerebrum and medial to the PLN (Figs. 4, 5a, b, 6a, b). The axon ascends ventrally to the CB but slightly posterior

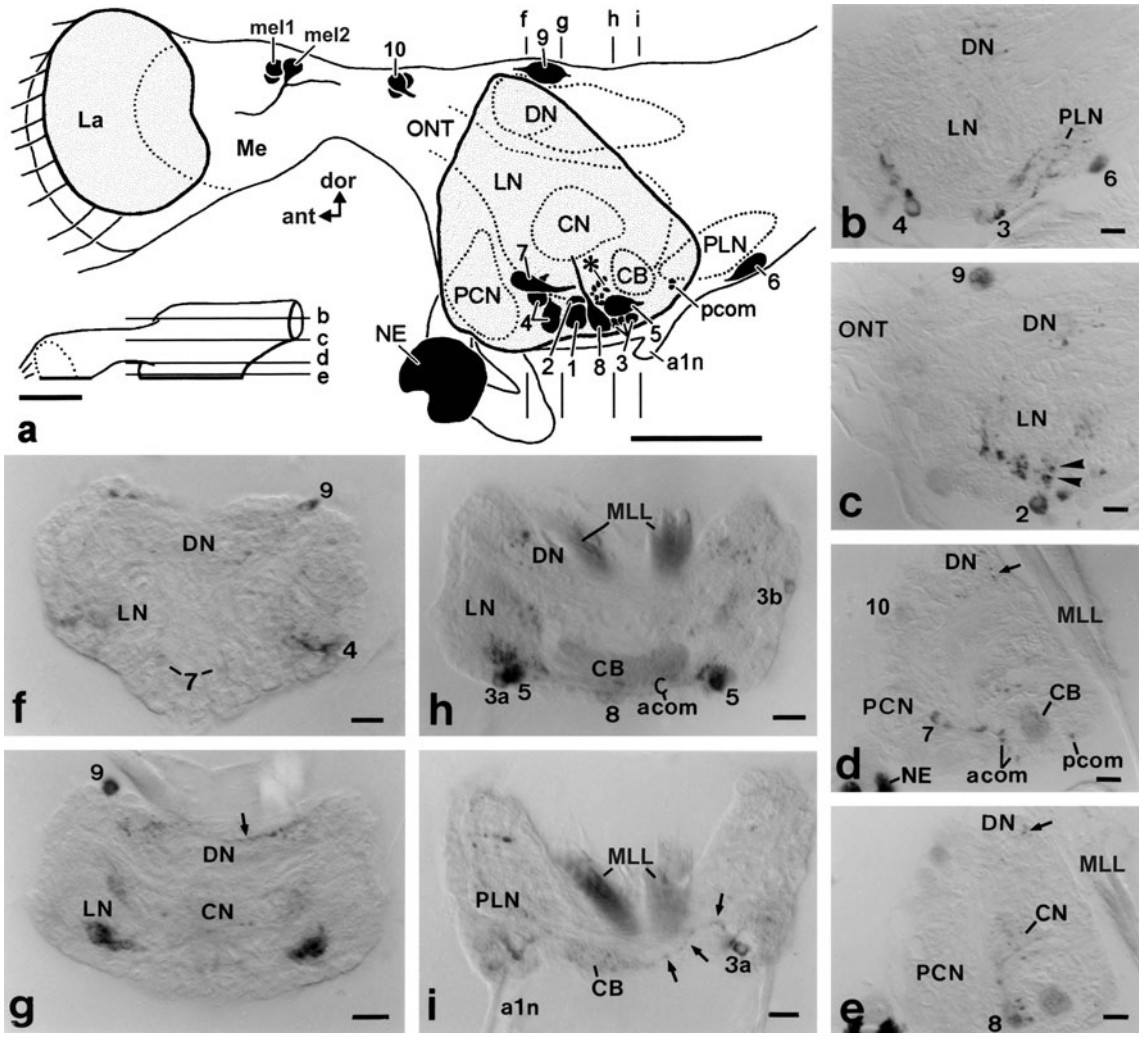

Fig. 6 PDH-ir neurons in Paraplast sections (15 µm thick) through the optic ganglia and the brain of *D. magna.* **a** Lateral view of a hemibrain showing the positions of the different neuron types relative to the brain neuropils as reconstructed from sagittal sections; note that the dorsal neuropil (*DN*) is laterally extended. Approximate planes of sagittal sections in **b–e** (*inset*: dorsal view of a hemibrain; the mid-sagittal plane is shown close to plane e and shaded in the lateral view above) and of cross sections in **f–i** are indicated; *ant* anterior, *dor* dorsal, *asterisk* indicates fibers in the anterior commissure. **b–e** Sagittal brain sections showing the positions of type-3, type-4, and type-6 neurons and fibers in the anterior ventral part of the lateral neuropil (*LN*) and in the postlateral neuropil (*PLN*, **b**), ventral type-2 and dorsal type-9 neurons and the origin of the fibers in the anterior commissure (*arrowheads*, **c**), the positions of the weakly stained type-7 neuron and its projection to the anterior commissure (*acom*, note also type-5 fibers in the posterior commissure *pcom; arrow* indicates type-9 axons; **d**), and the weakly stained type-8 neuron projecting into a plexus within the central neuropil (*CN*; *arrow* indicates type-9 axons, **e**). **f–i** Cross sections of the brain showing the positions of the weakly stained type-7, and the strongly stained type-4 and type-9 neurons and plexuses associated with the lateral (*LN*) and dorsal (*DN*) neuropils (**f**), the type-9 neuron at the dorsal margin of the protocerebrum, its contralateral axon (*arrow*) and the restricted fiber plexuses in the lateral (*LN*), central (*CN*), and dorsal (*DN*) neuropils with their lateral extensions (**g**); note the positions of the weakly stained cells of type-3a and type-3b and of the median type-8, the strongly stained type-5 neurons, the axons in the lower part of the *acom* ventral to the central body (*CB*, **h),** and the fibers entering the CB which obviously originate in type-3a neurons (*arrows*; **i**). Stefanini's fixation; PAP staining; *a1n* antennular nerve; *MLL* levator labri muscle; *ONT* optic nerve tract; for other abbreviations refer to Fig. 4. *Scale bars* 50 µm in **a**, all others 10 µm

to the type-5 neuron up to the anterior brain commissure where it splits into two branches. One branch crosses the midline via this commissure counter-parallel to the branch of the type-6 neuron of the other side and enters the contralateral LN. The other branch enters the ipsilateral LN (Figs. 4, 5d, e).

Type-7 neuron

This monopolar neuron characteristically shows a triangular or polygonal soma, which is localized in a mid-anterior ventral position just posterior to the PCN (Figs. 4, 5b, 6a, d, f). This neuron is always less intensely stained than the

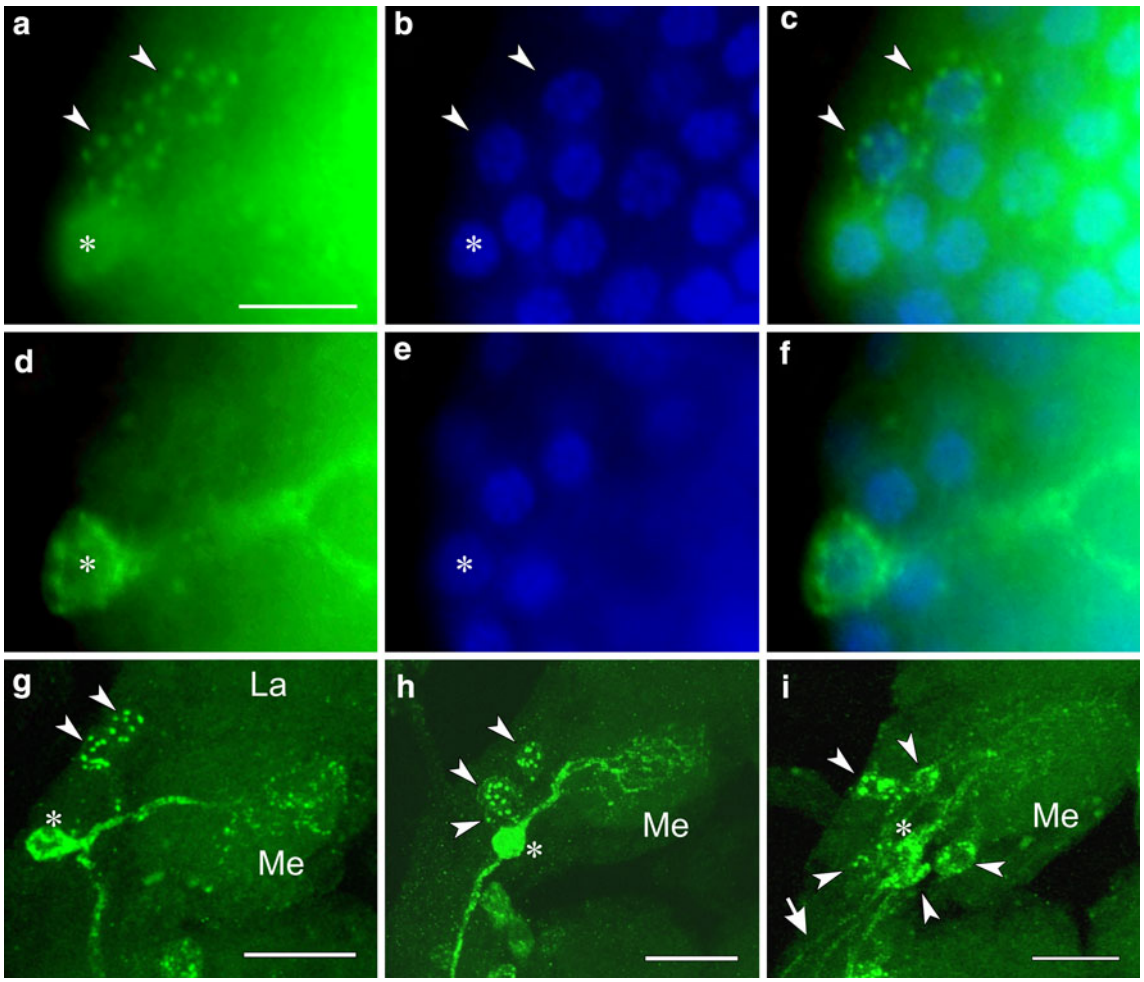

Fig. 7 Double staining of medulla lateral neurons with anti-PDH (**a**, **c**, **d**, **f**) and DAPI nuclear (**b**, **c**, **e**, **f**) staining. **a–c** mel1 neurons**,** single neurons and their nuclei are indicated by *arrowheads*; **d–f** mel2 neuron; soma indicated by *asterisk*s. Merged pictures show granular PDH-ir and nuclear staining belonging to single mel1- and mel2-somata (**c**, **f**). **g–i** mel1-and mel2-type neurons at different circadian times; note the most extreme changes in numbers and staining properties of mel1 neurons (*arrowheads*) at ZT 0 (**g**, 2 me1), ZT 6 (**h**, 3 mel1), and ZT 12 (**i**, 5 mel1) and the appearance of axons from bipolar mel1 neurons in the evening samples (*arrow* in **i**). Generally, a single mel2 neuron soma is present as indicated by *asterisk*; *La* lamina, *Me* medulla. *Scale bars* 10 µm in **a–f**, 20 µm in **g**–i

other neuron types mentioned above. In some preparations, it did not show any immunoreactivity. It projects caudally, and the axon bifurcates at the level of the anterior brain commissure; one branch turns ipsilaterally into the LN, where its traces are lost, the central branch is seen to enter the CB medially. In the *D. pulex* brain, this neuron is particularly prominent, and clearly innervates, in addition to the lateral neuropil and the CB, also the LNs (Fig. 5b); some fibres are bending backwards dorsally into the CN (not shown).

Type-8 neuron

This neuron type with a strongly stained and somewhat polygonally flattened to round soma and a faintly stained axon has only been detected in about half of the whole-mount preparations of *D. magna* BrOGs but occurred in all *D. pulex* BrOGs. The neuron is localized in the median-most position at the anterior ventral rim of the anterior brain commissure (Figs. 4, 5a, b, e, 6a, h), and its axon runs in a transversal and the mid-sagittal plane dorsally to terminals in the CNs as is obvious in mid-sagittal sections (Fig. 6a, e).

Type-9 neuron

This strongly stained bipolar neuron is the only immunopositive cell localized at the dorsal margin of the brain (Figs. 4, 5f, 6a). As revealed in most whole-mount preparations, the central axon crosses the midline in an oblique ventral direction and ramifies in the central and posterior lateral parts of the DN (Figs. 5a, b, f, 6d, e, h) extending into the tritocerebrum where the arborizations intermingle with branches of the lateral axon emerging from the contralateral bipolar neuron (Figs. 4, 5f, 6a, b–h).

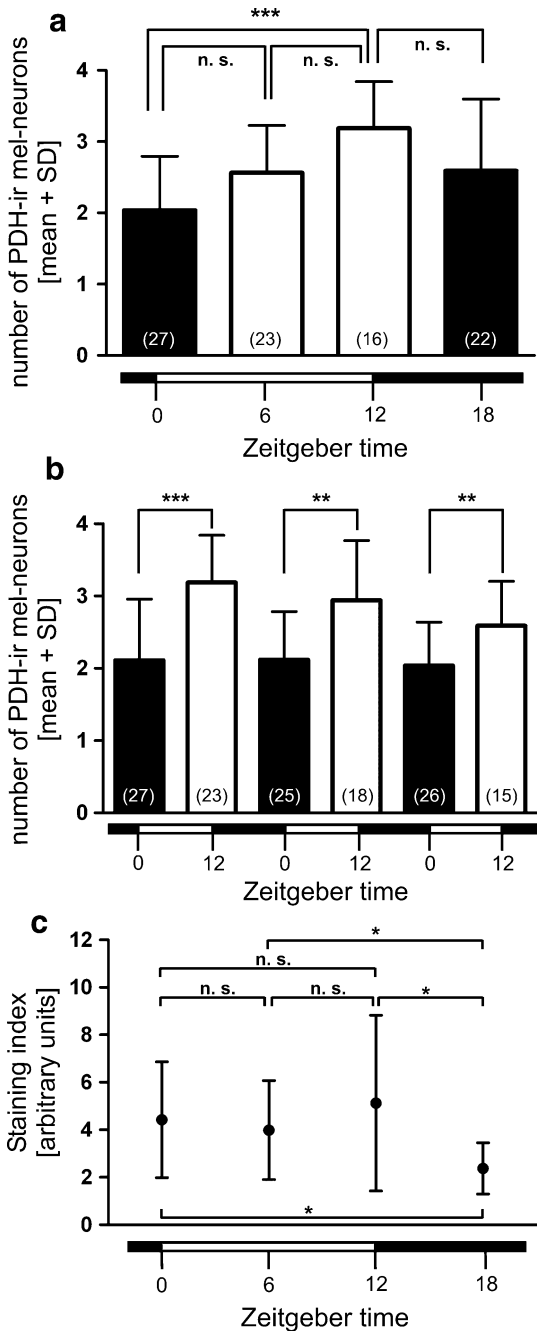

Fig. 8 Circadian rhythmicity in the mel1 neurons of *Daphnia magna* under 12:12 LD. Numbers of preparations evaluated for each time point are given in *parentheses*. **a** Diurnal changes in mel1 neuron numbers sampled at four different Zeitgeber time points (ZT) at 6-h intervals. After 12 h of dark phase, on average two mel1 neurons are present at ZT 0, after 12 h of light phase, three mel1 neurons are present ($p < 0.001$; Tukey's multiple comparison test). Neuron numbers at ZT 6 and ZT 18 show intermediate values, on average 2.56 mel1 neurons (ZT 6) and 2.59 (ZT 18), respectively. **b** The diurnal rhythm in mel1 neuron number is persistent over a time course of 3 days under 12:12 LD. Comparison of mel1 numbers at ZT 0 and ZT 12 consistently shows higher neuron numbers at the end of light phase. p values: Day 1, $p < 0.0001$; Day 2, $p = 0.001$; Day 3: $p = 0.0092$ (Student's t test). **c** Diurnal changes in the intensity of PDH-immunofluorescence as a measure of PDH neuron activity. Fluorescence intensity of mel1 neurons was summed from individual cells and a staining index was calculated as an average staining intensity, normalized to the maximum cell number to account for mel1 neuron number variations. The differences between intensity values from ZT 0, ZT 6, and ZT 12 are statistically not significant (n.s., $p > 0.05$) but staining intensity decreases significantly at ZT 18 compared with both ZT 12 ($p = 0.0216$), ZT 6 ($p = 0.0264$), and ZT 0 ($p = 0.0142$; Student's t test). Note that the changes in fluorescence intensity do not parallel the changes in neuron numbers. $n = 12$ for each time point

In *D. pulex* brains, this neuron type is usually very faintly stained.

Type-10 neuron

This type is localized as a group of up to three neurons next to the anterior dorsal and medial lateral margin of the brain (Figs. 5a–c, f, 6a, d) at its connection to the Me. It projects in posterior ventral direction most likely into the CN (Fig. 5f). The immunoreactivity is often so weak that it remains unrecognized.

Type-11 neuron

In the posterior medial lateral tritocerebrum at the level of the conspicuous first root of the second antenna nerve ($a2n_1$), one single monopolar neuron with elongated cell body occurs that branches profusely within the lateral tritocerebral neuropil and sends an axon into the circumesophageal neuropil where its traces are usually lost (Fig. 5g). Therefore, we cannot state with certainty whether its axon continues further down into the VNC. In some preparations, the neuron appeared totally absent without any relation to circadian times.

Circadian rhythmicity of mel1 neurons

Differences in total numbers of cell bodies of the distinct PDH-ir neuron types between the preparations were detected exclusively for the punctate-stained mel1 neurons (Figs. 7a–c, g–i), but not for the mel2 neurons (Figs. 7d–f, g–i). As *Daphniae* are isogenic organisms, genetic variation should not account for this variability between the specimens, but in fruit flies (*Drosophila melanogaster*) and other insects, a group of well-described clock neurons next to the medulla (the small LN_vs) changes its PDF activity and terminal morphology in the dorsal brain in a circadian manner [18, 56, 57]. The mel1-neuron numbers in *D. magna* varied significantly between the end of the dark phase (2.04 neurons ±0.146 SD, $n = 27$) and the end of the light phase (3.19 ± 0.16, $n = 17$; Figs. 7g–i, 8a). Thus, at the end of the light phase, on average one additional neuron is present. When applying one-way ANOVA, the

differences in neuron numbers between the time points are statistically highly significant ($p = 0.0002$, $F = 7.263$, $R^2 = 0.2060$, total ANOVA values: SS = 65.95, $df = 87$), while variances are not ($p > 0.05$, Bartlett's test). At the intermediate time points, i.e., at midday and midnight, the average neuron numbers lie between the values obtained at ZT 0 and ZT 12, indicating a time-dependent change in mel1-number. Multiple comparison tests showed highly significant differences between the time points at ZT 0 and ZT 12 ($p < 0.001$; Tukey's multiple comparison test). In these test, the average mel1 number between ZT 6 (2.57 ± 0.14, $n = 23$) and ZT 18 (2.59 ± 0.21, $n = 22$) did not differ ($p > 0.05$; Tukey's multiple comparison test). These findings suggests a mono-modal circadian change in the numbers of PDH-expressing mel1 neurons.

These diurnal changes in mel1-neuron numbers were confirmed over a period of 3 days for the time points at ZT 0 and ZT 12 (Fig. 8b). For all days, the difference in neuron number at ZT 0 and ZT 12 is statistically significant or highly significant (Student's t test; Day 1 $p < 0.0001$, $t = 4.360$, $df = 41$; Day 2 $p = 0.001$, $t = 3.556$; $df = 40$; Day 3 $p = 0.0092$, $t = 2.737$, $df = 40$). The time-dependency of changes in mel1 neuron number from this 3-day sample is statistically confirmed by two-way ANOVA ($p < 0.0001$; p values for other sources of variation were not statistically different; sum-of-squares = 26.89; mean squares = 26.89; $F = 58.32$). The average of two mel1 neurons is consistently found at ZT 0, while generally higher average mel1 numbers were found at ZT 12. However, the average number at ZT 12 was sometimes lower than three (see e.g., ZT 12 on day 3) and is, thus, more variable than the average number of two neurons at ZT 0.

Next, we tested if not only the neuron number, but also the PDH immunoreactivity in the neurons displays circadian changes. This was accomplished by quantifying the immunofluorescence intensity. Notably, the changes observed for the immunofluorescence intensity in cell bodies at ZT 0 and ZT 12 were not statistically significant ($p = 0.5883$, $t = 0.5494$, $df = 22$; Student's t test). However, the fluorescence intensity at midnight (ZT 18) clearly displayed a drop, which is statistically significant to the values obtained for lights-on ZT 0 ($p = 0.0142 < 0.05$, $t = 2.662$, $df = 22$), midday intermediate values ZT 6 ($p = 0.0264$, $t = 0.9297$, $df = 22$), and lights-off ZT 12 ($p = 0.0216 < 0.05$, $t = 2.474$, $df = 22$) (Fig. 8c). Thus, the activity rhythms in terms of peptide expression in the cell bodies appears to start some time before lights-off, stay high during daylight, but diminish significantly during night-time.

Furthermore, we investigated whether the oscillation in numbers of mel1 neurons continues under either constant light or constant darkness. If the diurnal variation of mel1 neurons is under endogenous control, we would expect the changes in neuron numbers to persist, and if they are regulated by light input, the differences in cell numbers between ZT 0 and ZT 12 should disappear under constant conditions between circadian time points (CT 0 and CT 12).

Under LL conditions, the circadian variation between CT 0 and CT 12 was established starting with a LD 12:12 control sampling ($p = 0.0012$, $t = 3.450$, $df = 47$, Student's t test) taken on the day prior to transfer to LL conditions (Fig. 9a). At day one under LL, this difference is continuously present ($p = 0.0079$, $t = 2.806$, $df = 38$, Student's t test). However, the average mel1-neuron number increases to 2.82 ± 0.14 ($n = 22$) at CT 0 on day three under LL, i.e., to a higher value than 2.39 ± 0.15 ($n = 23$) neurons at CT 0 on day one. Thereby, the difference in mel1-neuron numbers between CT 0 and CT 12 diminishes already over 3 days. Although the average mel1-neuron number is still slightly higher at CT 12 on day three, it no longer constitutes a significant difference ($p = 0.4646$, $t = 0.7377$, $df = 44$) as on day one. This minor difference in average mel1-neuron number persists even after 7 days ($p = 0.4717$, $t = 0.7246$, $df = 57$). This time series demonstrates that under LL conditions the mel1-neuron number reaches saturation. This state equals the average value at the end of the light period over 3 days and provides evidence for the dependence of the changes in mel1-neuron numbers upon light input.

Under DD conditions, the difference in mel1-neuron numbers between CT 0 and CT 12 remains statistically highly significant on day one ($p = 0.0003$, $t = 3.927$, $df = 46$, Student's t test) (Fig. 9b). On day three, the average number of mel1 neurons is lowered to 2.36 ± 0.26 ($n = 22$) at ZT 12. Accordingly, the numbers at CT 0 and CT 12 are still significantly different, but only to a lesser extent ($p = 0.036$, $t = 2.170$, $df = 40$). However, after 7 days, these diurnal changes have disappeared ($p = 0.6938$, $t = 0.3969$, $df = 35$).

Discussion

In this study, we report identification of a PDH of unusual primary structure, its precursor structures and its neuronal distribution in the nervous system in two water flea species. The reason for the unexpected complexity of PDH-ir neurons is far from clear, but we provide here the first demonstration that a subset of these neurons are not only highly similar to insect PDF-expressing clock neurons but also display endogenous circadian rhythmicity.

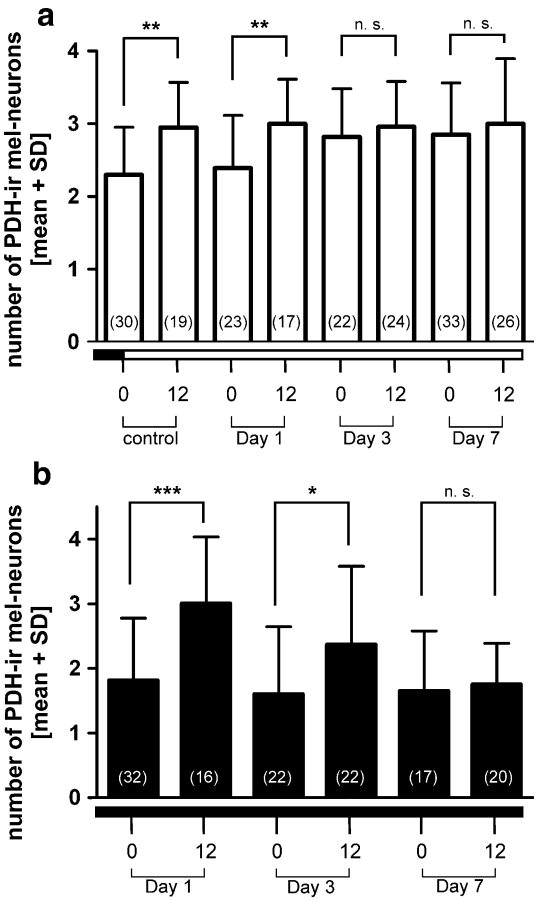

Fig. 9 Light drives the circadian changes in mel1 neuron numbers, as evidenced under regimes of continuous light (**a**) and continuous darkness (**b**). **a** Continuous light: the control shows the diurnal mel1 variation between an average of two mel1 neurons at circadian times CT 0 and three mel1 neurons at CT 12 prior to rearing animals under continuous light ($p = 0.0012$). The rhythmicity persists on day 1 ($p = 0.0079$), and is consecutively diminished as continuous light input raises the neuron number at CT 0 average of three mel1 neurons, with numbers becoming statistically not significant compared to CT 12 (Day 3, $p = 0.4646$; day 7, $p = 0.4717$). **b** Under constant darkness, diurnal variations of mel1-neuron numbers between CT 0 and CT 12 persist on day 1 ($p = 0.0003$) and are consecutively reduced as mel1–neuron numbers at CT 12 are lowered on day 3 ($p = 0.036$) and are no longer significantly different on day 7 ($p = 0.6938$; all Student's *t* test)

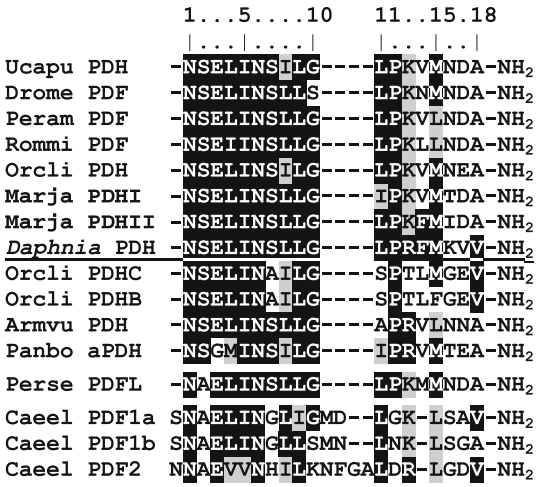

Fig. 10 Alignment of ecdysozoan pigment-dispersing hormones/factors (PDHs/PDFs), i.e., crustacean beta-PDHs of *Uca pugilator* (Ucapu PDH; Acc. No. 224648), *Orconectes limosus* (Orcli PDH, PDHB, PDHC, [62]), *Marsupenaeus japonicus* (Marja PDHI, PDHII, [61]), *Armadillidium vulgare* (Armvu PDH; Acc. No. BAI67599), and alpha-PDH of *Pandalus borealis* (Panbo PDH, [92]), insect PDFs of *Drosophila melanogaster* (Drome PDF, Acc. No. O96690), *Periplaneta americana* (Peram PDF, [93]), *Romalea microptera* (Rommi PDF, Acc. No. AAA90959), an onychophoran PDH from *Peripatopsis sedgwicki* (Perse PDH, Acc. No. FN235358), and three nematode PDFs from *Caenorhabditis elegans* (Caeel PDF1a, PDF1b, PDF2, [63]). Note the close relationship of *Daphnia* PDH (*underlined*) with Marja PDHII and the sharing of the rare C-terminal Val-NH_2 with Orcli PDHB, PDHC and Caeel PDF1a, PDF2. *Shading* indicates sequence identities (*black*) and similarities (*gray*) with *Daphnia* PDH

Identified precursor and peptide structures of an unusual *Daphnia* PDH

Although the ORF-derived precursors of both *Daphnia* species are very similar, the encoding nucleotide sequences show considerable differences (overall 58% identity only). Whereas the DapmaPDH mRNA has a shorter 3′-untranslated region than the putative DappuPDH precursor (Suppl. Fig. 1), the former is well in the range of other short PDH precursors, e.g., those of some penaeid shrimps and dipteran insects [58, 59]. The peptide-encoding parts differ only in three synonymous substitutions (Fig. 2b) not affecting the translated peptide sequences, which are identical in both species. When considering the entire translated ORFs, the precursor identities do not exceed 67%. The SPs are with 71.4% identical amino acid positions very similar, whereas the few similar stretches in the PPRP at best share a highest overall identity of 62% only. The latter property is commonly known from decapod PDH-precursors that also differ most within the PPRPs [2]. When comparing the *Daphnia* PDH peptide sequence itself with those of other known PDHs from malacostracans, primarily decapod crustaceans, and from insects, it is evident that the first 12aas have a typical beta-PDH signature including the apparently physiologically important and highly conserved "core" or "message" sequence of aas 6-9 [1, 2, 4, 60]; Fig. 10). This was most likely the reason for the clear detection of *Daphnia* PDH with our polyclonal antibodies against beta-type *Uca*-PDH that recognize a common epitope in the first 12aas of many decapod PDHs and insect PDFs [4, 5, 46]. However, among the last 6aas almost all are unusual except Met^{15}, which renders the peptide susceptible to sulfoxidation. This was likely the reason for detecting a small more hydrophilic and, therefore, earlier eluting immunoreactive peak in our HPLCs of

both the *Uca*-beta-PDH standard and the *Daphnia* PDH (Fig. 1). There was no evidence for the existence of another PDH-isoform as is known for several decapods. The last one-third of the *Daphnia* PDH-sequence is characterized by novel features combining two basic aas (Arg^{13}, Lys^{16}), leading to a strongly alkaline isoelectric point (IEP) of 8.75 (IEP of beta-PDH: 4.37), with three hydrophobic aas (Phe^{14}, Val^{17}, Val^{18}-amide). Thus, *Daphnia* PDH shares some rare properties such as the Phe^{14} with a shrimp *Marsupenaeus japonicus* PDH-II [61] and the Val^{18}-amide C-terminal with two out of three PDHs from the crayfish *Orconectes limosus* (Orcli-PDH-B: Phe^{15} and Val^{18}-amide, Orcli-PDH-C Val^{18}-amide; [62]). Interestingly, this rare C-terminal Val^{18}-amide is otherwise only known from two out of three recently discovered nematode PDFs (Caeel-PDF1a and -PDF2 [63]; Fig. 10). From extensive heterologous chromatophore bioassay studies in fiddler crabs using aa-substituted or truncated analogues of PDHs it is known that slight aa-exchanges at the C-terminal part (e.g., Asp^{17}, Glu^{17}) can have dramatic effects, depending on the targets, e.g., the different chromatophore cell types, tested [1, 4, 60]. Whereas the occurrence of Phe^{14} and the two C-terminal valines in *Daphnia* PDH could be explained as a result of single point mutations when compared to other beta-PDH mRNAs, the basic aas (Arg^{13}, Lys^{16}) would require two base exchanges per codon.

Our comparisons of peptide primary structures indicate a surprising degree of evolutionary divergence in an important peptide gene apparently widely distributed in Ecdysozoans incl. onychophorans and nematodes [63] (Fig. 10). For the two *Daphnia* species, the PDH itself has been conserved while the divergence in SPs and PPRPs is not surprising when considering their long separate evolutionary history [64].

Identified PDH-ir interneurons in the central nervous system

We found *Daphnia* PDH only in interneurons of the BrOG but not in typical neurosecretory neurons with neurohemal release sites. This situation is similar in the CNS of balanid and copepod crustaceans, in which also only PDH-ir interneurons occur [65, 66]. Interestingly, other cladoceran peptidergic neurons containing CHH, CCAP, and other peptides also occur only as interneurons in the CNS [36–38]. In decapod and isopod crustaceans, PDH-ir neurons also occur as interneurons involved, e.g., in visual information processing [5–10]. The apparent non-existence in cladocerans, balanids and copepods of neurohemal sinus glands, which in decapods are normally associated with chromatophorotropins and CHH-family peptides [5, 42, 67], has two possible explanations: either peptidergic interneurons evolved prior to humorally releasing neurosecretory neurons, or some neurohemal organs for peptidergic cells were reduced repeatedly in crustaceans.

Comparison of projection patterns and connectivities of *Daphnia* PDH-ir neurons with distinct neuropils in addition to their position and structure may allow some functional insights. Dendritic-like branches of the prominent contralaterally projecting PDH-ir type-2, -4, -5, -6 neurons heavily invade the LN where they may contact the mel2-neuron terminals and conduct left–right coordinations (Fig. 5c; see also below). The brain PDH-ir type-3, -5, -7 neurons are associated with the central body, a putative locomotory control centre as in insects. This suggests a novel modulatory role for *Daphnia* PDH. The neuropil DN (Figs. 4, 5f, 6a), discussed previously as a protocerebral bridge (PB) in cladocerans ("Dorsal area" [50]), is poorly innervated by PDH-ir fibres. It is thus perhaps functionally less relevant than comparable PB neuropiles in decapods or similar dorsal neuropile areas in insects that are involved in circadian PDH/PDF signaling [20, 68]. The PB is in two crayfish species the main innervation site of extra-retinal photoreceptors where they likely contact PDH-ir-descending interneurons assumed to drive circadian locomotory patterns [20]. In *Daphnia* brains, only the tritocerebral type-11 neurons have similar positions and projection patterns but do not descend down the VNC as in decapods. Physiologically, however, this seems unnecessary since the motoneurons responsible for the swimming locomotion of *Daphnia* driven by the large second antennae are likely located within the tritocerebrum only, as is well known for antennal motoneurons of crayfish [69].

Ample evidence from classical histology for neurosecretory cells being restricted to the brains of *D. pulex* and *D. magna* (but without associated neurohemal release sites) has been provided for some dorso-frontal neurons (up to four ventral groups) and some neurons in the circumesophageal connectives [32–34, 70]. The type-1 PDH-ir brain neurons give rise to short and swollen bulb-like terminals extending into the PLNs. These characters are typical for the third group of cells in the ventral brain surface region III described earlier [70]. This suggests that parts of these putative neurosecretory neurons are interneurons exhibiting synaptic-like or paracrine release of PDH as a neuromodulator. Furthermore, it would be interesting to establish whether any of the *Daphnia* PDH-ir neuron types 1–5, 7–8 and 11 are members of the ventral and esophageal/tritocerebral putative neurosecretory cell groups, that have previously been suggested to be involved in the control of moulting and egg-deposition [71]. The fact that type-11 neurons were not observed in all preparations may be due to changes in their activity during the moult cycle.

It is surprising that earlier studies using classical neurosecretory cell-specific staining did not reveal such cells

in the optic ganglia of cladocerans. However, the medulla-associated PDH-ir mel-interneurons of *Daphnia* can be compared in terms of positions and projection patterns, i.e., (1) anteriorly to the Me and/or the La and (2) posteriorly into the protocerebrum (see also below), with several *Daphnia* neurons described and illustrated earlier as T neurons [52, 54, 72]. Retzius [72] described two small adjacent bipolar neurons in the lateral medulla of *D. magna* that exhibit branches in the La, the Me, and the ipsilateral LN of the brain. These neurons resemble the mel1 neurons. Furthermore, he reconstructed another larger bipolar neuron next to the Me that closely resembles the mel2 neurons. This large neuron also closely resembles a Golgi-impregnated tangential T neuron in the lateral medulla of *D. magna* that connects the La and the Me with the LN of the brain [54]. This connectivity is a typical structural feature of wide-field lateral PDF-clock neurons in many insects [12].

Circadian activity rhythms in PDH-ir mel1 neurons of *D. magna*

We provide here evidence for the *D. magna* mel1 neurons showing robust circadian changes in numbers: there are on average more active PDH-ir mel1 neurons at the end of the light phase than at the end of the dark phase. The change in numbers of PDH-expressing mel1 neurons raises questions about whether (1) the absolute mel1-neuron number is changing, or whether (2) the expression, translation, and release of PDH in a fixed number of neurons are dynamically regulated under circadian control. Continuous light leads to a saturation effect for the observed recruitment of active mel1 neurons because PDH expression increases to the regular number (max. 5) at the end of the light phase, whereas constant darkness limits the number of active neurons to a minimum of two. We cannot exclude that the two canonical mel1 neurons have functions different from the additional three dynamically regulated mel1 neurons. Since mel1 neurons are unlikely to arise de novo every day and in such a short time, we suppose that translation and thus immunoreactivity of PDH in mel1-cell bodies (and possibly their release activity) follows a circadian rhythm, visible as the recruitment of certain cells in this group dramatically changing their PDH-ir. Since this rhythmicity had disappeared under constant LL and DD conditions after 7 days of observation, this rhythm is dependent upon photic input, although we cannot say whether dependence is direct or indirect. However, for 3 days under constant conditions, the circadian changes in mel1-neuron numbers were significant, albeit in decline (Fig. 9b). This finding is thus indicative of a substantial circadian (i.e., endogenous) component underlying the rhythmic variation in mel1-neuron number. If the rhythm were entirely free-running, a phase shift would be expected, as circadian rhythms are usually not perfect 24 h cycles. However, a clarification of this issue would need finer time resolution than our 12 h intervals. On the other hand, if the diurnal variation of mel1-neuron numbers were solely controlled by light input, it would have disappeared immediately under DD conditions.

Circadian oscillatory secretory dynamics are best known for the expression of CHH-ir in decapod XOSG-neurosecretory cells, albeit only comprising a constant total number of CHH-ir cells, and for concentrations of the CHH peptide in the hemolymph [73–75]. Since the PDH-ir mel1 neurons are located in almost identical positions between different specimens, we assume that these cells, which are dynamically regulated under LL and DD continuous conditions, belong to a limited pool. Thus, the cycling of PDH-ir most likely represents highly dynamic changes in translation, production and release of PDH in mel1 neurons. As some mel1 neurons seem to lose their PDH-ir entirely at ZT 0, this appears to be a novel and extreme case of short-term down-regulation of neuropeptide expression in a putative clock neuron.

The significant changes in fluorescence intensity (as standardized via the staining index; Fig. 8c) are not exactly synchronous with the changes in mel1 numbers. However, as the fluorescence intensity at ZT 0 had obviously increased already in the darkness when compared to ZT 18, this is indicative of an anticipatory increase in PDH-expression prior to the onset of the light phase. Interestingly, similar observations have been made for rhythmical changes in both activity and plasticity of the terminals of the PDF-ir small LNvs in the dorsal brain neuropils of *D. melanogaster*. These changes not only involved cycling of PDF-immunoreactivity [18] but also morphological remodeling of terminal shape, length and bouton sizes interpreted as indicative of rhythmic PDF-release [57]. Although, in *D. magna*, we have quantified the cell bodies only, similar activity rhythms might exist in axons and terminals of mel1 neurons because their stainability was also higher in evening (ZT 12) preparations (see Fig. 7i).

Comparative aspects of putative clock neuron homology

Many aspects of crustacean biology follow a circadian rhythm driven by endogenous biological clocks. However, the identification of clock neurons satisfying criteria for autonomous pacemakers has not been easily forthcoming in any of the crustacean models investigated so far [17, 76, 77]. *Daphnia* and other cladoceran species have, as per many other planktonic organisms, developed escape strategies among which a light-entrained circadian behavior

known as diel vertical migration (DVM) in the water body is probably the most important [78–81]. Furthermore, many other diel rhythmic and photoperiod-dependent behaviours are known for cladoceran species such as circadian eye-pigment movements, growth and reproductive diapause control [82–85]. In *Daphnia*, an endogenous biological clock is known to exist from behavioural analysis of the DVM [86], but the neuronal control of this behavior is not known. The PDH-system is the prime candidate for a circadian clock control system in crustaceans because it is central to circadian regulation and conserved during evolution of insects and malacostracans [9,17].

In most insects, the prominent lateral PDF-ir clock neurons are located adjacent to the optic lobes usually next to the medulla or the accessory medulla neuropil (AcMe; [12, 13, 87–89]). We did not find any association of mel- or other PDH-ir neurons with structures reminiscent of an AcMe-like neuropil. However, comparative studies have shown that PDH-ir neurons are located next to the medulla in several crustacean species [6, 9, 10] and their numbers are usually higher than in *Daphnia*. In the visual ganglia of the lobster *H. americanus,* putative insect PDF neuron homologues occur in the PDH-ir subgroups C′–C‴ [9]. These subgroups correspond to the much simpler and clearly distinguishable *Daphnia* mel1 and mel2 neurons that are even easier to compare with the *Drosophila* PDF neurons regarding positions, projection patterns, and PDH-immunoreactivity than the decapod PDH neurons: The mel1 neurons not only are morphologically and qualitatively similar to s-LN_vs but also show circadian activity patterns that resemble the rhythmic activity of s-LN_vs, albeit with a different acrophase in the evening [18, 57]. The mel2 neurons connecting the optic ganglia and the brain are highly similar to l–LN_vs, which project to the contralateral medulla and connect the two brain hemispheres [90]. While such contralateral projections of the mel2 neurons could not be established in the present work, they cannot be ruled out. Functionally, left–right synchronizing connections could also be brought about via a network with other contralaterally projecting PDH-ir type-2, -4, -5, -6 neurons putatively contacting mel2-neuron projections in the LN. The projections of *Drosophila* s-LN_vs to the dorsal brain are similar to the axonal projection patterns of the mel1 neurons to the *Daphnia* brain DNs that were detectable only in the evening (Fig. 7i). In the DNs, the mel1 neurons may even contact the PDH-ir type-9 neurons that contralaterally connect the DN and the PLNs next to the tritocerebrum (Figs. 4, 5f, 7i).

The presence of two similar PDH-ir neuron types exclusively associated with the medulla in Branchiopoda and Diptera may reflect distinct specializations of the respective clades. Homologous PDH-ir neurons in the optic ganglia may occur as synapomorphies of Pancrustacea, but not necessarily as two distinct classes of pacemaker clock neurons. *Daphnia,* thus, presents a unique model for the study of homologies between crustacean PDH- and insect PDF-expressing neuron types due to the relatively low number of mel neurons compared to decapods. Furthermore, the highest diurnal activity of the clearly rhythmically active PDH-ir mel1 neurons is observed in the evening and at night, which coincides well with the highest locomotory activity related to the DVM and feeding behaviour. Thus, it seems likely that the mel neurons function as clock neurons linking the PDH oscillations to a behavioural rhythm. This link makes it promising to explore the PDH neurons in more depth as putative first elements of a biological clock in *Daphnia*. Water fleas as models for ecologically important water organisms are now particularly promising for knock-down experiments, since the *D. pulex* genome contains the ancient antiviral RNA interference genes producing the necessary set of enzymes such as Argonaute and Dicer for processing of double stranded RNA [91].

Acknowledgments The Carl Tryggers Foundation, Stockholm, Sweden (to J.S. and H.D.), the Faculty of Sciences, Stockholm University (to H.D.), the Federal ministry for research and technology, Germany (BMFT, to Q.Z.), and postdoctoral research grants from the Fund for Scientific Research—Flanders, Belgium (F.W.O.-Vlaanderen, to P.V., J.H., K.P.), and the German Research Foundation (DFG to R.P.) are gratefully acknowledged by the authors. We are greatly indebted to Achim Stommel, State office for nature, environment, and customer protection, North-Rhine Westphalia (LaNUV), Bonn, Germany, for providing *Daphnia magna* and green algae stocks and many useful rearing advises. The authors also wish to thank Dr. S.G. Webster, University of North Wales, Bangor, UK for his generous gift of synthetic *Uca*-beta-PDH. The authors wish to thank our facility manager Dr. Stina Höglund, Wenner-Gren Institute, Stockholm University, for technical help with confocal microscopy, and Dr. Anthony Poole, Department of Molecular Biology and Functional Genomics, Stockholm University, for help with final stylistical polishing of the text.

References

1. Rao KR, Riehm JP (1993) Pigment-dispersing hormones. Ann NY Acad Sci 680:78–88
2. Rao KR (2001) Crustacean pigmentary-effector hormones: chemistry and functions of RPCH, PDH, and related peptides. Am Zool 41(3):364–379
3. Rao KR, Mohrherr CJ, Riehm JP, Zahnow CA, Norton S, Johnson L, Tarr GE (1987) Primary structure of an analog of crustacean pigment-dispersing hormone from the lubber grasshopper *Romalea microptera*. J Biol Chem 262(6):2672–2675
4. Rao KR, Riehm JP (1989) The pigment-dispersing hormone family: chemistry, structure-activity relations, and distribution. Biol Bull 177:225–229
5. Dircksen H, Zahnow CA, Gaus G, Keller R, Rao KR, Riehm JP (1987) The ultrastructure of nerve endings containing pigment-dispersing hormone (PDH) in crustacean sinus glands: identification by an antiserum against synthetic PDH. Cell Tissue Res 250:377–387

6. Mangerich S, Keller R, Dircksen H, Rao KR, Riehm JP (1987) Immunocytochemical localization of pigment-dispersing hormone (PDH) and its coexistence with FMRFamide-immunoreactive material in the eyestalks of the decapod crustaceans *Carcinus maenas* and *Orconectes limosus*. Cell Tissue Res 250:365–375
7. Hsu Y-WA, Stemmler EA, Messinger DI, Dickinson PS, Christie AE, de la Iglesia HO (2008) Cloning and differential expression of two beta-pigment-dispersing hormone (beta-PDH) isoforms in the crab *Cancer productus*: evidence for authentic beta-PDH as a local neurotransmitter and beta-PDH II as a humoral factor. J Comp Neurol 508(2):197–211
8. Mangerich S, Keller R (1988) Localization of pigment-dispersing hormone (PDH) immunoreactivity in the central nervous system of *Carcinus maenas* and *Orconectes limosus* (Crustacea), with reference to FMRFamide immunoreactivity in *O. limosus*. Cell Tissue Res 253(1):199–208
9. Harzsch S, Dircksen H, Beltz BS (2009) Development of pigment-dispersing hormone-immunoreactive neurons in the American lobster: homology to the insect circadian pacemaker system? Cell Tissue Res 335(2):417–429
10. Nussbaum T, Dircksen H (1995) Neuronal pathways of classical crustacean neurohormones in the central nervous system of the woodlouse, *Oniscus asellus* (L). Phil Trans R Soc Lond B 347:139–154
11. Helfrich-Förster C (1995) The *period* clock gene is expressed in central nervous system neurons which also produce a neuropeptide that reveals the projections of circadian pacemaker cells within the brain of *Drosophila melanogaster*. Proc Natl Acad Sci USA 92(2):612–616
12. Helfrich-Förster C (2005) Organization of endogenous clocks in insects. Biochem Soc Trans 33(5):957–961
13. Homberg U, Reischig T, Stengl M (2003) Neural organization of the circadian system of the cockroach *Leucophaea maderae*. Chronobiol Int 20(4):577–591
14. Tomioka K, Matsumoto A (2010) A comparative view of insect circadian clock systems. Cell Mol Life Sci 67(9):1397–1406. doi:10.1007/s00018-009-0232-y
15. Helfrich-Förster C, Stengl M, Homberg U (1998) Organization of the circadian system in insects. Chronobiol Int 15(6):567–594
16. Meinertzhagen IA, Pyza E (1996) Daily rhythms in cells of the fly's optic lobe: taking time out from the circadian clock. Trends Neurosci 19(7):285–291
17. Strauß J, Dircksen H (2010) Circadian clocks in crustaceans: identified neuronal and cellular systems. Front Biosci 15:1040–1074
18. Park JH, Helfrich-Förster C, Lee G, Liu L, Rosbash M, Hall JC (2000) Differential regulation of circadian pacemaker output by separate clock genes in *Drosophila*. Proc Natl Acad Sci USA 97(7):3608–3613. doi:10.1073/pnas.070036197
19. Zavodska R, Wen C-J, Hrdy I, Sauman I, Lee H-J, Sehnal F (2008) Distribution of corazonin and pigment-dispersing factor in the cephalic ganglia of termites. Arthropod Struct Dev 37:273–286
20. Sullivan JM, Genco MC, Marlow ED, Benton JL, Beltz BS, Sandeman DC (2009) Brain photoreceptor pathways contributing to circadian rhythmicity in crayfish. Chronobiol Int 26(6):1136–1168. doi:10.1080/07420520903217960
21. Ståhl F (1938) Preliminary report on the colour changes and the incretory organs in the heads of some crustaceans. Ark Zool 30 B 8:1–3
22. Zaffagnini F (1987) Reproduction in *Daphnia*. In: Peters RH, De Bernardi R (eds) *Daphnia*. Memoria dell' Istituto Italiano di Idrobiologia Dott. Marco de Marchi vol 45. Verbania Pallanza, Italy: Istituto Italiano di Idrobiologia, pp 245–284
23. Koshida Y, Hiroki M (1980) *Artemia* as a multipurpose biomaterial for biology education. In: Persoone G, Sorgeloos PM, Roels OEJ (eds) The brine shrimp *Artemia*. Universa Press, Wetteren, pp 289–298
24. Fingerman M (1985) The physiology and pharmacology of crustacean chromatophores. Am Zool 25(1):233–252
25. Gard AL, Lenz PH, Shaw JR, Christie AE (2009) Identification of putative peptide paracrines/hormones in the water flea *Daphnia pulex* (Crustacea; Branchiopoda; Cladocera) using transcriptomics and immunohistochemistry. Gen Comp Endocrinol 160(3):271–287
26. Colbourne JK, Eads BD, Shaw J, Bohuski E, Bauer DJ, Andrews J (2007) Sampling *Daphnia*'s expressed genes: preservation, expansion and invention of crustacean genes with reference to insect genomes. BMC Genomics 8:217. doi:10.1186/1471-2164-8-217
27. Eads BD, Andrews J, Colbourne JK (2008) Ecological genomics in *Daphnia*: stress responses and environmental sex determination. Heredity 100(2):184–190. doi:10.1038/sj.hdy.6800999
28. Tatarazako N, Oda S (2007) The water flea *Daphnia magna* (Crustacea, Cladocera) as a test species for screening and evaluation of chemicals with endocrine disrupting effects on crustaceans. Ecotoxicology 16(1):197–203. doi:10.1007/s10646-006-0120-2
29. Persoone G, Baudo R, Cotman M, Blaise C, Thompson KCl, Moreira-Santos M, Vollat B, Törökne A, Han T (2009) Review on the acute *Daphnia magna* toxicity test—evaluation of the sensitivity and the precision of assays performed with organisms from laboratory cultures or hatched from dormant eggs. Knowl Managt Aquatic Ecosyst 393:01
30. LeBlanc GA (2007) Crustacean endocrine toxicology: a review. Ecotoxicology 16(1):61–81
31. Barata C, Alanon P, Gutierrez-Alonso S, Riva MC, Fernandez C, Tarazona JV (2008) A *Daphnia magna* feeding bioassay as a cost effective and ecological relevant sublethal toxicity test for environmental risk assessment of toxic effluents. Sci Total Environ 405(1–3):78–86. doi:10.1016/j.scitotenv.2008.06.028
32. Sterba G (1957) Die neurosekretorischen Zellgruppen einiger Cladoceren (*Daphnia pulex* und *magna*, *Simocephalus vetulus*). Zool Jahrb Anat 76:303–310
33. Halcrow K (1969) Sites of presumed neurosecretory activity in *Daphnia magna* Straus. Can J Zool 47:575–577
34. Van den Bosch de Aguilar P (1972) Les charactéristiques tinctoriales des cellules neurosécrétrices chez *Daphnia pulex* (Crustacea:Cladocera). Gen Comp Endocrinol 18:140–145
35. Montagné N, Desdevises Y, Soyez D, Toullec JY (2010) Molecular evolution of the crustacean hyperglycemic hormone family in ecdysozoans. BMC Evol Biol 10. doi:10.1186/1471-2148-10–62
36. Zhang Q, Keller R, Dircksen H (1993) Immunocytochemical mapping of peptidergic neurons in the nervous system of *Daphnia magna* (Crustacea; Cladocera). In: Elsner N, Heisenberg M (eds) Genes-brain-behaviour. Thieme, Stuttgart, p 545
37. Zhang Q, Keller R, Dircksen H (1997) Crustacean hyperglycaemic hormone in the nervous system of the primitive crustacean species *Daphnia magna* and *Artemia salina* (Crustacea: Branchiopoda). Cell Tissue Res 287(3):565–576
38. Zhang Q, Dircksen H (1999) Immunocytochemical mapping of crustacean cardioactive peptide in the nervous system of *Daphnia magna* and *Artemia salina* (Crustacea: Cladocera, Anostraca). Comp Biochem Physiol 124A:S86
39. Dircksen H, Zhang Q (2006) Neuropeptide-containing neurons in the central nervous system of the waterflea *Daphnia magna*. Comp Biochem Physiol 143A:S118
40. Van Harreveld A (1936) A physiological solution for freshwater crustaceans. Proc Soc Exp Biol Med 34:428–432

41. Stefanini M, De Martino C, Zamboni L (1967) Fixation of ejaculated spermatozoa for electron microscopy. Nature 216:173–174
42. Dircksen H, Webster SG, Keller R (1988) Immunocytochemical demonstration of the neurosecretory systems containing putative moult-inhibiting and hyperglycemic hormone in the eyestalk of brachyuran crustaceans. Cell Tissue Res 251:3–12
43. Boer HH, Schot LPC, Roubos EW, ter Maat A, Lodder JC, Reichelt D, Swaab DF (1979) ACTH-like immunoreactivity in two electronically coupled giant neurons in pond snail *Lymnaea stagnalis*. Cell Tissue Res 202:231–240
44. Hall TA (1999) BioEdit: a user-friendly biological sequence alignment editor and analysis program for Windows 95/98/NT. Nucl Acids Symp Ser 41:95–98
45. Löhr J, Klein J, Webster SG, Dircksen H (1993) Quantification, immunoaffinity purification and sequence analysis of a pigment-dispersing hormone of the shore crab, *Carcinus maenas* (L.). Comp Biochem Physiol B 104(4):699–706
46. Honda T, Matsushima A, Sumida K, Chuman Y, Sakaguchi K, Onoue H, Meinertzhagen IA, Shimohigashi Y, Shimohigashi M (2006) Structural isoforms of the circadian neuropeptide PDF expressed in the optic lobes of the cricket *Gryllus bimaculatus*: immunocytochemical evidence from specific monoclonal antibodies. J Comp Neurol 499(3):404–421
47. Sternberger LA (1974) Immunocytochemistry. Prentice Hall Inc., Englewood Cliffs, NJ
48. Dircksen H, Müller A, Keller R (1991) Crustacean cardioactive peptide in the nervous system of the locust, *Locusta migratoria*: an immunocytochemical study on the ventral nerve cord and peripheral innervation. Cell Tissue Res 263:439–457
49. Rieger D, Shafer OT, Tomioka K, Helfrich-Förster C (2006) Functional analysis of circadian pacemaker neurons in *Drosophila melanogaster*. J Neurosci 26(9):2531–2543. doi:10.1523/JNEUROSCI.1234-05.2006
50. Aramant R, Elofsson R (1976) Distribution of monoaminergic neurons in the nervous system of non-malacostracan crustaceans. Cell Tissue Res 166(1):1–24
51. Cunnington WA (1903) Studien an einer Daphnide, *Simocephalus sima*. Beiträge zur Kenntnis des Centralnervensystems und der feineren Anatomie der Daphniden. Jena Z Naturwiss 37:447–520
52. Leder H (1915) Untersuchungen über den feineren Bau des Nervensystems der Cladoceren. Arb Zool Inst Univ Wien u Triest 20:297–392
53. Binder G (1932) Das Muskelsystem von *Daphnia*. Int Rev ges Hydrobiol Hydrograph 26:54–111
54. Nässel DR, Elofsson R, Odselius R (1978) Neuronal connectivity patterns in the compound eyes of *Artemia salina* and *Daphnia magna* (Crustacea: Branchiopoda). Cell Tissue Res 190(3): 435–437
55. Strausfeld NJ, Nässel DR (1980) Neuroarchitecture of brain regions that subserve the compound eyes of Crustacea and insects. In: Autrum H (ed) Handbook of sensory physiology, vol VII/6b: comparative physiology and evolution of vision in invertebrates. Springer, Berlin Heidelberg New York, pp 1–133
56. Helfrich-Förster C (1993) Pigment-dispersing hormone-immunoreactive neurons in the nervous system of wild-type *Drosophila melanogaster* and of several mutants with altered circadian rhythmicity. J Comp Neurol 337(2):177–190
57. Fernandez MP, Berni J, Ceriani MF (2008) Circadian remodeling of neuronal circuits involved in rhythmic behavior. PLoS Biol 6(3):e69. doi:10.1371/journal.pbio.0060069
58. Ohira T, Tsutsui N, Kawazoe I, Wilder MN (2006) Isolation and characterization of two pigment-dispersing hormones from the whiteleg shrimp, *Litopenaeus vannamei*. Zool Sci 23(7):601–606
59. Park JH, Hall JC (1998) Isolation and chronobiological analysis of a neuropeptide pigment-dispersing factor gene in *Drosophila melanogaster*. J Biol Rhythms 13(3):219–228
60. Rao KR, Riehm JP (1988) Pigment-dispersing hormones: a novel family of neuropeptides from arthropods. Peptides 1:153–159
61. Yang WJ, Aida K, Nagasawa H (1999) Characterization of chromatophorotropic neuropeptides from the kuruma prawn *Penaeus japonicus*. Gen Comp Endocrinol 114(3):415–424
62. Bulau P, Meisen I, Schmitz T, Keller R, Peter-Katalinic J (2004) Identification of neuropeptides from the sinus gland of the crayfish *Orconectes limosus* using nanoscale on-line liquid chromatography tandem mass spectrometry. Mol Cell Proteomics 3(6):558–564
63. Janssen T, Husson SJ, Meelkop E, Temmerman L, Lindemans M, Verstraelen K, Rademakers S, Mertens I, Nitabach M, Jansen G, Schoofs L (2009) Discovery and characterization of a conserved pigment-dispersing factor-like neuropeptide pathway in *Caenorhabditis elegans*. J Neurochem 111(1):228–241. doi:10.1111/j.1471-4159.2009.06323.x
64. Lehman N, Pfrender ME, Morin PA, Crease TJ, Lynch M (1995) A hierarchical molecular phylogeny within the genus *Daphnia*. Mol Phylogenet Evol 4(4):395–407. doi:10.1006/mpev.1995.1037
65. Webster SG (1998) Peptidergic neurons in barnacles: an immunohistochemical study using antisera raised against crustacean neuropeptides. Biol Bull 195(3):282–289
66. Sousa GL, Lenz PH, Hartline DK, Christie AE (2008) Distribution of pigment-dispersing hormone- and tachykinin-related peptides in the central nervous system of the copepod crustacean *Calanus finmarchicus*. Gen Comp Endocrinol 156(3):454–459. doi:10.1016/j.ygcen.2008.03.008
67. Mangerich S, Keller R, Dircksen H (1986) Immunocytochemical identification of structures containing putative red pigment-concentrating hormone in two species of decapod crustaceans. Cell Tissue Res 245:377–386
68. Yasuyama K, Meinertzhagen IA (2010) Synaptic connections of PDF-immunoreactive lateral neurons projecting to the dorsal protocerebrum of *Drosophila melanogaster*. J Comp Neurol 518(3):292–304. doi:10.1002/cne.22210
69. Sandeman DC, Wilkens LA (1983) Motor control of movements of the antennal flagellum in the Australian crayfish, *Euastacus armatus*. J Exp Biol 105:253–273
70. Angel MV (1967) A histological and experimental approach to neurosecretion in *Daphnia magna*. In: Stutinsky F (ed) Neurosecretion. Springer, Berlin Heidelberg New York, pp 230–237
71. Van den Bosch de Aguilar P (1969) Nouvelles données morphologiques et hypothèses sur le rôle du système neurosécréteur chez *Daphnia pulex* (Crustacea: Cladocera). Ann Soc Roy Zool Belg 99 (1–2):27–44
72. Retzius G (1906) Zur Kenntnis des Nervensystems der Daphniden. Biol Unters N F 13:107–116
73. Gorgels-Kallen JL, Voorter CEM (1985) The secretory dynamics of the CHH-producing cell group in the eyestalk of the crayfish, *Astacus leptodactylus*, in the course of the day/night cycle. Cell Tissue Res 241:361–366
74. Kallen JL, Abrahamse SL, van Herp F (1990) Circadian rhythmicity of the crustacean hyperglycemic hormone (CHH) in the hemolymph of the crayfish. Biol Bull 179:351–357
75. Fanjul-Moles ML, Escamilla-Chimal EG, Salceda R, Giulianini PG, Sanchez-Chavez G (2010) Circadian modulation of crustacean hyperglycemic hormone in crayfish eyestalk and retina. Chronobiol Int 27(1):34–51
76. Aréchiga H, Rodriguez-Sosa L (2002) Distributed circadian rhythmicity in the crustacean nervous system. In: Wiese K (ed) The crustacean nervous system. Springer, Berlin Heidelberg New York, pp 113–122

77. Fanjul-Moles ML, Prieto-Sagredo J (2003) The circadian system of crayfish: a developmental approach. Microsc Res Tech 60:291–301
78. Dini ML, Carpenter SR (1992) Fish predators, food availability and diel vertical migration in *Daphnia*. J Plankton Res 14(3):359–377
79. Makino W, Haruna H, Ban S (1996) Diel vertical migration and feeding rhythm of *Daphnia longispina* and *Bosmina coregoni* in Lake Toya, Hokkaido, Japan. Hydrobiologia 337(1–3):133–143
80. Young S, Watt PJ (1996) Daily and seasonal vertical migration rhythms in *Daphnia*. Freshwater Biol 36(1):17–22
81. Ringelberg J (1999) The photobehaviour of *Daphnia* spp. as a model to explain diel vertical migration in zooplankton. Biol Rev Cambridge Phil Soc 74(4):397–423
82. Rammner W (1929) Über periodische Erscheinungen am Cladoceren-Individuum (Häutung, Fortpflanzung, Wachstum). Internat Rev Ges Hydrobiol u Hydrograph 21(5/6):402–420
83. Sed'a J (1992) Diurnal periodicity in *Daphnia* reproduction. Hydrobiologia 246(2):119–127
84. Stross RG (1996) Significance of photoperiodism and diapause control in the multicycle crustacean *Daphnia pulex* Leydig. Hydrobiologia 320:107–117
85. Cellier-Michel S, Berthon JL (2003) Rhythmicity of the pigments in the compound eye of *Daphnia longispina* (Cladocera). J Freshw Ecol 18(3):445–450
86. Ringelberg J, Seruaas H (1971) A circadian rhythm in *Daphnia magna*. Oecologia 6(3):289–292
87. Helfrich-Förster C (1998) Robust circadian rhythmicity of *Drosophila melanogaster* requires the presence of lateral neurons: a brain-behavioral study of disconnected mutants. J Comp Physiol [A] 182(4):435–453
88. Sehadova H, Sauman I, Sehnal F (2003) Immunocytochemical distribution of pigment-dispersing hormone in the cephalic ganglia of polyneopteran insects. Cell Tissue Res 312:113–125
89. Helfrich-Förster C (2009) Neuropeptide PDF plays multiple roles in the circadian clock of *Drosophila melanogaster*. Sleep Biol Rhythms 7:130–143
90. Helfrich-Förster C (2003) The neuroarchitecture of the circadian clock in the brain of *Drosophila melanogaster*. Microsc Res Tech 62(2):94–102
91. McTaggart SJ, Conlon C, Colbourne JK, Blaxter ML, Little TJ (2009) The components of the *Daphnia pulex* immune system as revealed by complete genome sequencing. BMC Genomics 10:175. doi:10.1186/1471-2164-10-175
92. Fernlund P (1976) Structure of a light-adapting hormone from the shrimp, *Pandalus borealis*. Biochim Biophys Acta 439(1):17–25
93. Mohrherr CJ, Rao KR, Riehm JP (1991) Characterization of a pigment-dispersing factor from the American cockroach. Soc Neurosci Abstr 17:276